Horizon 2020

Societal Challenge: Improving the air quality and reducing the carbon footprint of European cities

Project: 690105 – ICARUS

Full project title:

Integrated Climate forcing and Air pollution Reduction in Urban Systems

D3.5 Technical report on the evaluation of the changes in the surface radiative forcing due to implementation of mitigation strategies at local level

WP3- Integrated atmospheric modelling for connecting pressures to the environment to concentrations at the regional and urban scales

Lead beneficiary: Fondazione CMCC

Date: October 2019

Nature: Report

Dissemination level: PU

TABLE OF CONTENTS

Document Information

Grant Agreement Number	690105	**Acronym**	ICARUS
Full title	Integrated Climate forcing and Air pollution Reduction in Urban Systems		
Project URL	http://icarus2020.eu/		
Project Officer	Mirjam Witschke - Mirjam.WITSCHKE@ec.europa.eu		

Delivery date	**Contractual**	October 2019	**Actual**	October 2019
Status	Draft ☐		Final X	
Nature	Demonstrator ☐	Report X	Prototype ☐	Other ☐
Dissemination level	Confidential ☐	Public X		

Responsible Author (Partners)	**Fondazione CMCC**			
Responsible Author	Enrico Scoccimarro		**Email**	enrico.scoccimarro@cmcc.it
	Partner	CMCC	**Phone**	+39 051 0301609
Other partners (Institution)	AUTH			

Document History

Name (Institution)	Date	Version
CMCC	September 2019	Version 1
AUTH	October 2019	Version 2
CMCC	October 2019	Final

1 Introduction

The aim of this document is the evaluation of the changes in the surface radiative forcing associated to the aerosols due to implementation of mitigation strategies at local level based on the methodology described in ICARUS Milestone MS17 and applied to data described in ICARUS Milestone MS20.
The Characterization of aerosol in terms of global warming potential is suggested through the application of a simplified scheme that translates different types of Aerosols Optical Depth (AOD) changes into a first order assessment of radiative forcing. This will be done assigning a surface Radiative forcing change (ΔF) to changes in Aerosols Optical Depth (AOD) associated to different species, based on the Chylek and Henderson (2003) method. The availability of a CMCC present climate simulation at the global scale, based on a fully Coupled General Circulation Model with an aerosol module implemented within its atmospheric component, give us the possibility to verify the consistency between changes in vertically integrated aerosols concentrations and the relative changes in AOD, associated to mitigation strategies, as provided by WP2 and WP3 (see deliverable D3.3). Also the CMCC model will provide a measure of the interannual variability of the AOD associated to different species, useful to compare the magnitude of the changes induced by the mitigation strategies implemented within ICARUS over the designed cities.

2 The ΔF estimate

The term "radiative forcing" has been defined by the Intergovernmental Panel on Climate Change (IPCC) to represent an externally imposed perturbation in the radiative energy budget of the Earth's climate system. Such a perturbation can be brought by changes that affect the radiative energy absorbed by the surface (e.g., changes in surface reflection properties). This imbalance in the radiation budget has the potential to lead to changes in climate parameters and thus result in a new equilibrium state of the climate system. The radiative forcing (ΔF) of the surface-troposphere system due to the perturbation in or the introduction of an agent (i.e. a change in greenhouse gas concentrations) is the change in net irradiance (solar plus long-wave; in [Wm−2]). In the context of climate change, the term forcing is restricted to changes in the radiation balance of the surface troposphere system imposed by external factors, with no changes in stratospheric dynamics.

Radiative forcing is a useful tool for a first order estimate of the relative climate impacts due to radiatively induced perturbations. The practical appeal of the radiative forcing concept is due, in the main, to the assumption that there exists a general relationship between the global mean forcing and the global mean equilibrium surface temperature response (i.e., the global mean climate sensitivity parameter, λ). This parameter is similar for all the different types of forcings. With an approximate near invariance of λ of the order of about 25%.

Based on the assumption that:

$$\frac{\Delta T_S}{\Delta F} = \lambda \qquad \text{eq.1}$$

Based on tipical values of λ (0.5 k/wm-2 +-25%), it is possible to derive ΔTs (surface temperature variations values that we can expect based on the different radiative forcing parameter (ΔF) considered. Such ΔF parameter strongly depends on the considered species and simplified approaches conducted to a series of formulas to derive ΔF from species concentrations We consider table 6.2 in IPCC 5th Assessment Report (https://www.ipcc.ch/report/ar5/), chapter 6 for the present work, but an additional effort must be made for the derivation of ΔF associated to changes in aerosols concentration.

The impact of aerosols on the magnitude of incoming and outgoing solar radiation in the atmosphere and, therefore, Earth's climate, is largely determined by their optical properties. The optical properties of aerosols are crucial for evaluating their effect on radiative forcing and are dictated by the relative humidity, wavelength of incident light, and aerosol chemical and physical properties, especially size.

In order to obtain ΔF values associated to changes in the AOD expected for each of the considered aerosols species, based on the different mitigation strategies, we leverage on Chylek and Henderson (2003) formulation, defined within a theoretical study investigating uncertainty in aerosol optical properties, defined as:

$$\begin{aligned}\Delta F &= \frac{\partial F}{\partial \tau}\Delta\tau \\ &= -2\frac{S_0}{4}T^{+}T^{-}(1-N)\left[(1-a)^2\beta\omega - 2a(1-\omega)\right]\Delta\tau.\end{aligned}$$

eq.2

where: $\Delta\,\tau$ = change in aerosol optical depth (AOD),

S_0 = 1368 W/m-2, T+ T_ = 0.80, N = 0.5, a = 0.2 for the land and a = 0.05 for the ocean, b = 0.20 and w = 0.95, from which we obtain dF /dt = 29 for the land and dF /dt = 46 over the ocean.

3 The Models involved in the analysis

The CMCC General Circulation Model

Under the World Climate Research Programme (WCRP) the Working Group on Coupled Modelling (WGCM) established the Coupled Model Intercomparison Project (CMIP) as a standard experimental protocol for studying the output of coupled atmosphere-ocean general circulation models (AOGCMs). CMIP provides a community-based infrastructure in support of climate model diagnosis, validation, intercomparison, documentation and data access. This framework enables a diverse community of scientists to analyze GCMs in a systematic way. CMCC participated to the last CMIP effort (the CMIP5) with a bunch of GCMs, at different horizontal resolution and with different implementations. The CMCC model used in this study is an atmosphere-aerosol-ocean-sea ice coupled model consisting of ECHAM5 as atmospheric component, OPA 8.2 as oceanic component, LIM2 as sea ice model, and the HAM module for aerosols [D'Errico et al. 2015]. interactively coupled (namely, the CMCC aerosol climate model). The software used to couple the atmosphere (including the aerosols) and the ocean components is OASIS3. Basically, the atmosphere-ocean-sea ice coupled components are the same of the state-of-the-art CMCC-CM coupled model [Scoccimarro et al., 2011; Fogli et al., 2009], but here the atmosphere is at lower resolution and interactively coupled with an aerosol module. In this study ECHAM5 is used with six shortwave radiation bands [Cagnazzo et al., 2007] and a horizontal resolution at triangular truncation T63 with 31 vertical levels and the top of the atmosphere at 10 hPa. OPA8.2 is a primitive equation ocean general circulation model that is numerically solved on a global ocean curvilinear grid known as ORCA [Madec and Imbard, 1996]. Here we use ORCA2, with a resolution of 2° of longitude and a variable mesh of 0.5–2° of latitudes from the equator to the poles. The vertical grid has 31 levels (the 31st level is below the bottom) with variable layer depth and a constant 10m step in the top 100 m. The aerosol module HAM has a prognostic representation of the composition, size distribution, and mixing state of the major global aerosol components: sulphate, black carbon (BC), particulate organic matter, sea salt, and mineral dust (DU) [Stier et al., 2005, 2007]. The module predicts the evolution of an ensemble of microphysically interacting internally and externally mixed aerosol populations. The lifetime is estimated as the ratio of the column burden to the total source: the BC lifetime is 5.4 days and the lifetime for DU is 4.6 days as reported in Stier et al. [2005] (their Table 5). The scheme for dust emissions is based on Tegen et al. [2002, 2004], while that of sea-salt emissions is based on Schulz et al. [2004]. For black and organic matter, fossil fuel and biofuel [Bond et al., 2004], vegetation fires [Van Der Werf et al., 2003], and biogenic emissions are used. The aerosol properties generated from the ECHAM5-HAM coupling have been analyzed in detail in previous works: the model is able to simulate anthropogenic aerosol concentrations and aerosol optical depths reasonably well [Folini and Wild, 2011; Henriksson et al., 2011; Stier et al., 2005, 2007]. In this study the aerosol single scattering albedo, i.e., the ratio of the extinction due to scattering to the total extinction due to scattering and absorption, is derived from Aerosol Robotic Network.

A long simulation representing the present climate has been conducted, with oceanic initial conditions derived from a stable control simulation (about a thousand of years). For ICARUS purposes we aim to analyze the last 35 years of this experiment with external forcings kept constant (fixed to conditions typical for the year 2000). Forcings include the concentrations of well-mixed green-house gases and incoming solar irradiance for year 2000 from the CMIP5 forcing data. The seasonally varying ozone distribution is repeated every year and is based on the 2000 year climatology. For aerosols, the emission data set is based on the Aerosol Comparisons between Observations and Models (AeroCom) aerosol model intercomparison project inventories for the year 2000 [Dentener et al., 2006].

Due to the low horizontal resolution of the aforementioned model, the representation of the averaged values around the selected ICARUS cities will be based on few grid points.

The relationship between temperature and aerosols concentrations (or/and AOD) will be investigated also in terms of interannual variability based on monthly anomalies covering the entire 35 period. As a preliminary example, Figure 1/2/3 represent the interannual variability of SO4/Black Carbon/Organic Carbon, compared to the temperature over Athens as resulting from CMCC model. Upper panel represents the temperature time series anomaly and the central and lower panels represent burden concentration and optical depth respectively.

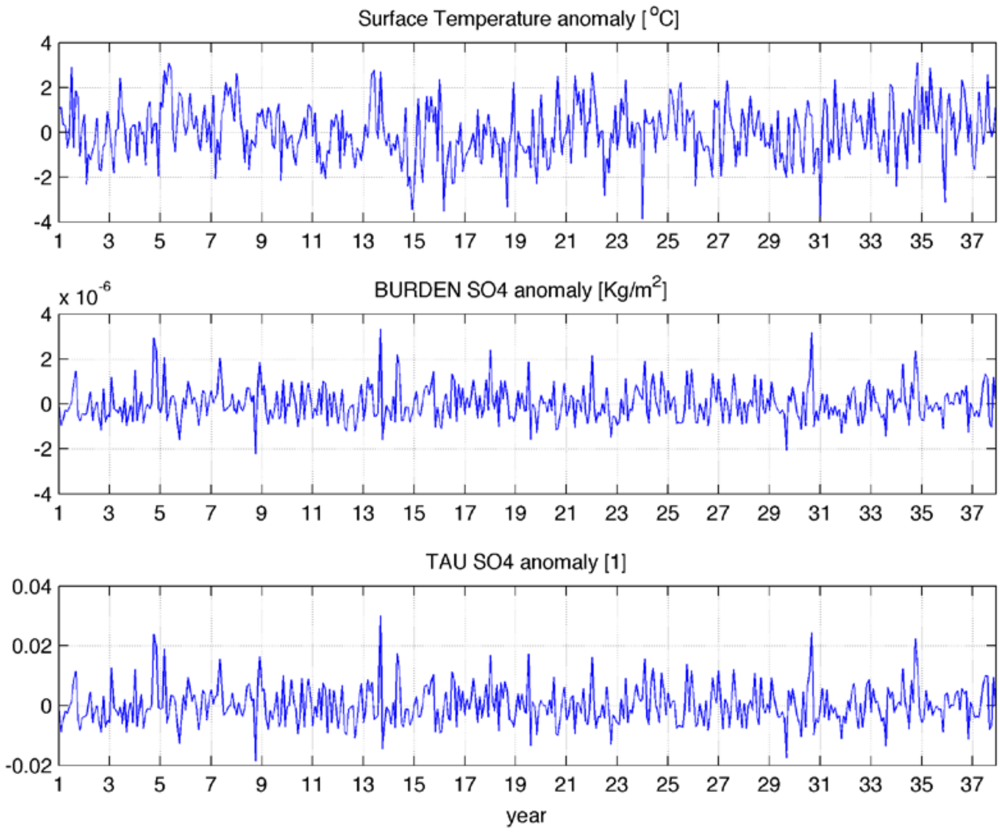

Figure 1: Anomalies of air temperature (1st atmospheric level, upper panel), Burden SO4 (central panel) and SO4 Optical Depth (lower panel) over the city of Athens as represented by CMCC model.

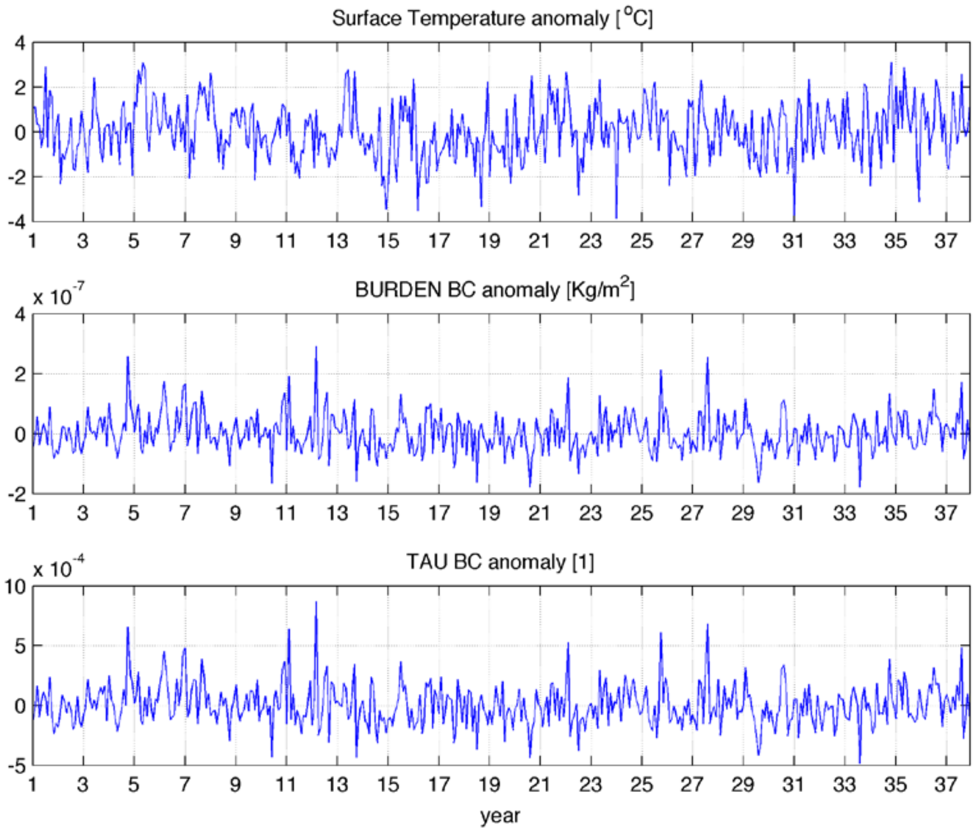

Figure 2: Anomalies of air temperature (1st atmospheric level, upper panel), Burden Black Carbon (central panel) and Black Carbon Optical Depth (lower panel) over the city of Athens as represented by CMCC model.

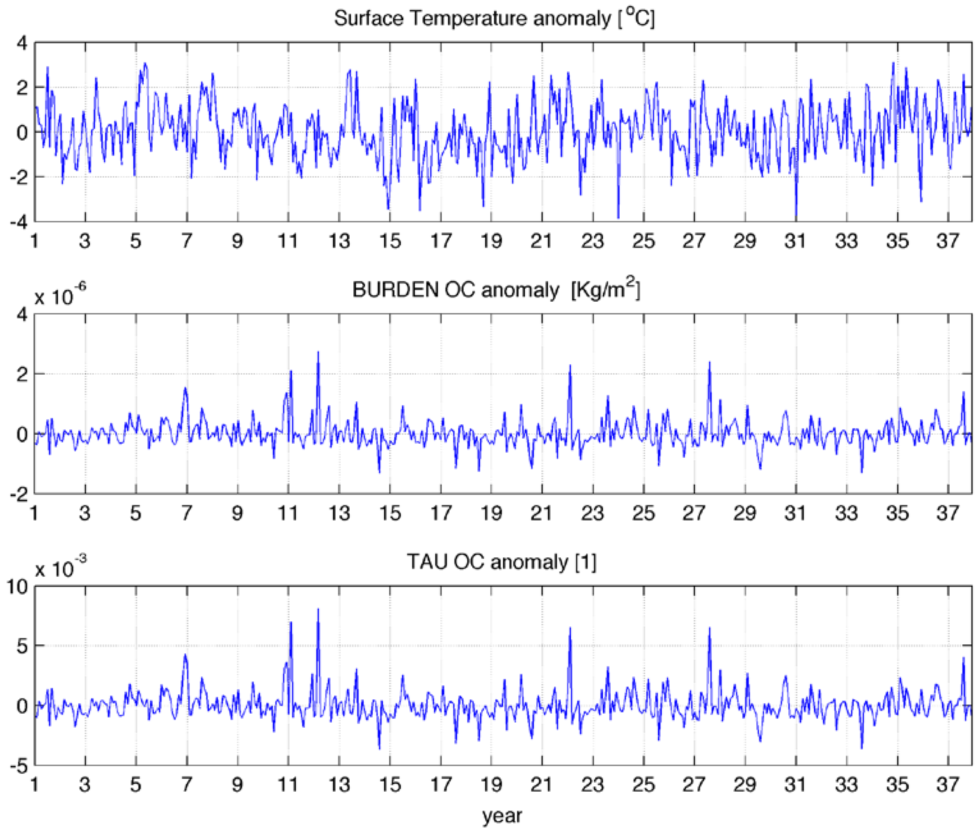

Figure 3: Anomalies of air temperature (1st atmospheric level, upper panel), Burden Organic Carbon (central panel) and Organic Carbon Optical Depth (lower panel) over the city of Athens as represented by CMCC model.

The CMCC COSMO-MFS Regional Model

In case of significant differences in the radiative forcing induced by the ICARUS mitigation strategies over the selected cities, the CMCC COSMO-MFS Regional Climate model will be used to perform targeted simulation (10 years around the selected year) with the aim to dynamically verify the induced effect on surface temperature.

The CMCC COSMO-MFS (Cavicchia et al. 2014, 2016) is the one contributing to the MedCORDEX (https://www.medcordex.eu/) simulations with a set of regional models implemented in the Mediterranean region. Specifically, the COSMOCLM, limited area atmospheric model can be employed in standalone mode or used in coupled mode with the oceanic model NEMO implemented in the Mediterranean basin. COSMOCLM (Rockel et al. 2008) is the climate version of the COSMO model (Steppeler et al. 2003), the operational nonhydrostatic mesoscale weather forecast model developed at the German Weather Service (DWD). Successively, the model has been modified by the CLMCommunity, in order to develop also climatic applications. The updates of its dynamical and physical packages allow its application in cloud resolving scales (Doms and Forstner 2004). It can be used with a spatial resolution between 1 and 50 km. For more details on the formulation of the model and on the parameterization settings, the reader is addressed to (Holton 2004 ; Tiedtke 1989). In the present version of the coupled AORCM, the atmospheric component COSMOCLM is implemented with a spatial resolution of about 0.44 (about 44 km) and 40 vertical levels. The spatial domain covers the Mediterranean region, including an Atlantic box, ranging from 54W67E and 8.75N63.75N (Figure 4). The choice of the domain is justified by the need to cover the Mediterranean basin region, including an area over the eastern part of the Atlantic Ocean (Atlantic box), which is necessary to the coupling with the Mediterranean Sea model. The ocean component of the system is NEMOMFS, a regional configuration of Nucleus for European Modelling of the Ocean (NEMO; Madec 2008) implemented at very high resolution in the Mediterranean basin. As it has been shown in Oddo et al. (2009). NEMOMFS is an eddy permitting marine model able to represent the dynamical processes that characterize the Mediterranean Sea. In the present configuration of the coupled AORCM, NEMOMFS has a 1/16_ (about 6.7 km) horizontal resolution and 71 levels along the vertical.

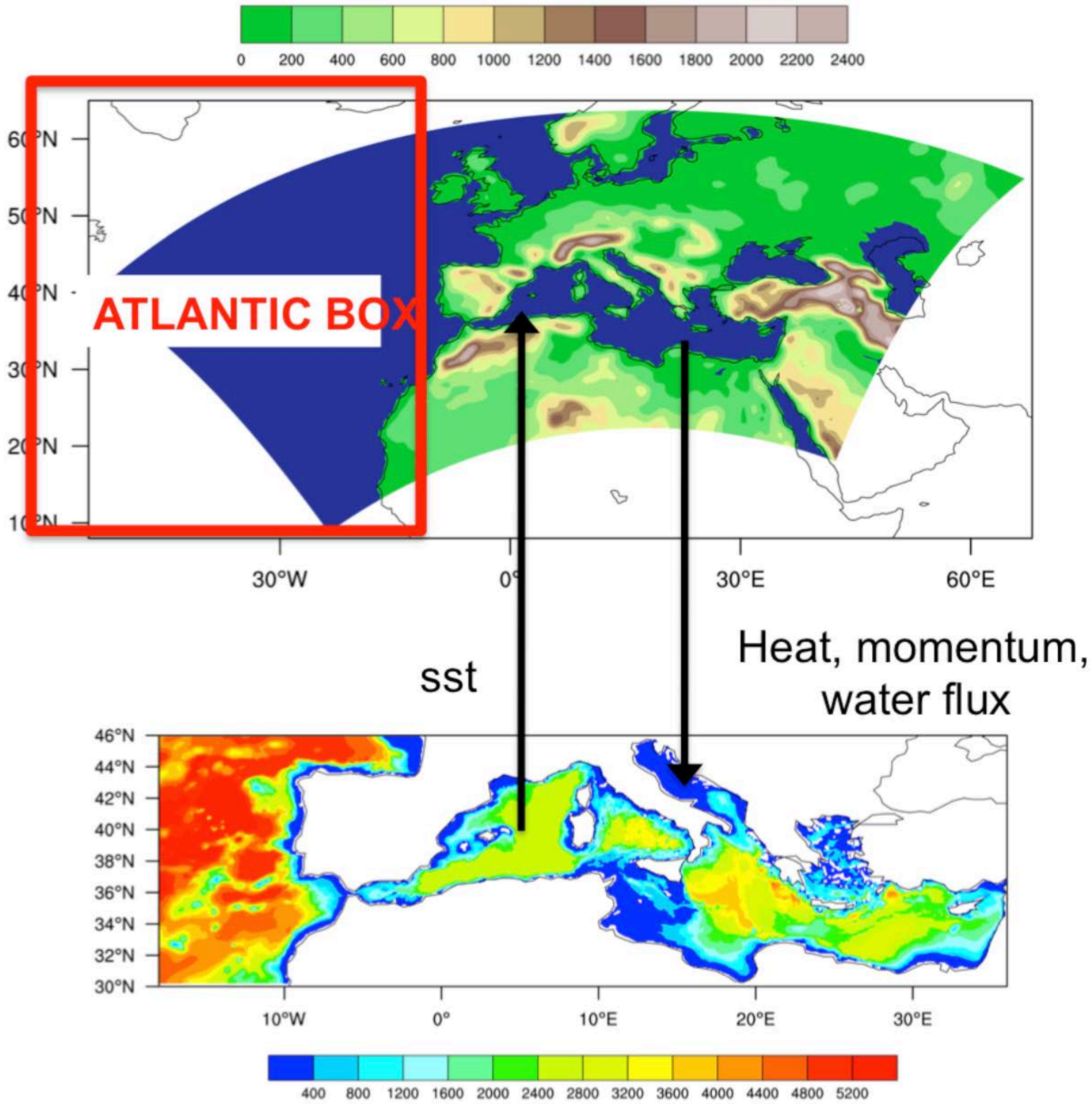

Figure 4: CMCC COSMO-MFS model components and domain.

The WRF-Chem Regional Climate Model

WRF-Chem is used for high resolution atmospheric modeling over ICAURS cities. The model details are listed in Milestone M3.2 and the simulation setup in Deliverable D3.3. In summary, WRF-Chem is the Weather Research and Forecasting (WRF) model coupled with a Chemistry component. The model simulates the emission, transport, mixing, and chemical transformation of trace gases and aerosols simultaneously with the meteorology. The model is used for investigation of regional-scale air quality, field program analysis, and cloud-scale interactions between clouds and chemistry. The WRF-Chem (version 3.6.1, August 2014) has been used for the present studies. For the simulations the meteorological data from NCAR/UCAR database (RCP4.5), including variables, such as Air Temperature, Boundary Layer Winds Geopotential Height, were downloaded. For the emission inventory both EDGAR HTAP V2 and the University of Stuttgart (USTUTT) High Resolution Emission Inventory Data were used.

The option of two level multiple horizontal nesting has been adopted. An outer grid with dimensions 12x12km has been implemented over Europe as shown in Figure 3.5. The Grid Projection has been defined as Lambert conformal Conic with lat0 = 35° lat1=65° standard lat=52° standard long= 10° consisting of 303 x 303 cells. On the urban scale nine (9) nests with dimensions 2x2km have been used consisting of 42x42 grid cells each. The cities/domains considered are: Thessaloniki, Stuttgart, Milano, Madrid, Ljubljana, Copenhagen, Brno, Basel, Athens.

Simulation period cover the years 2001-2050 by selecting Representative Days which were derived from the Weather Clustering analysis. Table 1 presents the selected RDs of Thessaloniki, for three 5-year periods and for three clusters (clusters with the most elevated pollution levels). The same methodology was used for the rest ICARUS cities as it is described in detail in D3.3. Aerosol Optical Depth and temperature data have been collected for all of the nine domains/periods simulated for each grid cell (42x42=1764 cells) at the daily time frequency over the periods indicated in table 1 defined based on D3.3 cluster definition . All of the mentioned data-set are already available through the ftp CMCC server and available for the ICARUS community as described in chapter 4.

Period	**Cluster 2 (NO2)**	**Cluster 4 (O3)**	**Cluster 7 (PM)**
2016-2020	2016-01-16	2017-07-21	2019-11-04
2021-2025	2022-02-25	2021-09-03	2023-11-05
2031-2035	2031-02-17	2033-07-20	2034-02-24

Table 1. Periods to be considered for the present deliverable analysis. Same as D3.3 table 4.3.8.

4 Data availability

In addition to the climate data set already made available for ICARUS partners, we provided the air quality model results from WRF-Chem used as an input for the current analysis on the same FTP site. This has been done for each of the modelled ICARUS domains (as defined in D3.3).

Together with aerosols data from CMCC-CM General Circulation Model (as listed in Appendix 1), aerosol optical depth data from WRF-Chem high resolution simulations are available through the CMCC ftp server (download.cmcc.bo.it – user and password sent privately to the ICARUS partners reference person).

The data format used is, where possible, NetCDF (http://www.unidata.ucar.edu/software/netcdf/). NetCDF is an abstraction that supports a view of data as a collection of self-describing, portable objects that can be accessed through a simple interface. Array values may be accessed directly, without knowing details of how the data are stored. Auxiliary information about the data, such as what units are used, are stored with the data. Generic utilities and application programs can access NetCDF datasets and transform, combine, analyze, or display specified fields of the data.

5 Results over the ICARUS cities

Based on the clustering analysis described in D3.3, different periods have been simulated at the high horizontal resolution over the ICARUS cities, using the WRF-Chem model under different climate forcing conditions. Provided boundary conditions are used to downscale to the city level through the WRF-Chem (version 3.6.1, August 2014) model over ICARUS cities (Thessaloniki, Stuttgart, Milano, Madrid, Ljubjana, Copenaghen, Brno, Basel, Athens). The option of two level multiple horizontal nesting has been adopted. An outer grid with dimensions 12x12km has been implemented over Europe On the urban scale nine (9) nests with dimensions 2x2km have been used consisting of 42x42 grid cells each. As from D3.3 different periods have been selected over the different cities for comparison between radiative forcing associated to future (about 2035) and present (about 2018) AOD after the application of ICARUS mitigation strategies.

It is important to stress that the present analysis describes the metodological approach to perform the required analysis on the impact on the local climate induced by mitigation strategies in terms of aerosols emission reduction. Anyway, the short period simulated (due to computational limitations) around each considered date, at the highest resolution with the WRF-Chem model adopting changes in aerosols emissions, is not sufficient to realistically represent climate conditions over the region: a longer period would be necessary to give significance to the repesentativeness of the presented results.

The evaluation of the changes in the radiative forcing as resulting from mitigation strategies linked to changes in Aerosols Optical Depth is described in chapter 2 and is based on data gathered (and available on the CMCC ftp server for ICARUS partners) within the MS20. Results for each city are shown in the current chapter.

As already mentioned the changes (future wrt present) in Aerosols effects over ICARUS cities is provided in terms of differences in the total Aerosol Optical Depths values over the modelled 2kmX2km resolution domains, comparing such difference with the interannual AOD variability of the CMCC-CM model (35 years obtained after a long present climate spinup) over the same city. The ΔF estimate between future and past is computed and its significance is evaluated based on a Montecarlo approach at the 5% level building on of the series of numbers provided by the CMCC-CM model over the 35y period considered. Also, the temperature change resulting from the ΔF estimate is then compared to the interannual variability of CMCC-CM modelled temperature over the same domain). This is performed based on winter and summer periods, defining winter and summer differently (different months considered) for the different cities, since the simulate short period at the high resolution over the cities is not the same but depends on the cluster approach defined in D3.3.

Next paragraphs shows the aforementioned results city by city. For the definition of the simulated periods relative to winter and summer, over each city, the reader can refer to deliverables D3.3.

Thessaloniki

Thessaloniki is the domain where we tested the planned methodology for the first time. Figure 5 shows the dimension and position of the WRF-Chem modelled domain. Reinforcing the aforementioned assumption that more extended simulated periods is necessary for a significant analysis on the potential changes that AOD modifications might induce on the regional climate, Figures 6 and 7 show that, together with a different spatial AOD distribution over the domain, the interannual variability of such parameter is not negligible during both seasons. A higher AOD during the intermediate year considered (2025/2021 for winter/summer), compared to 2018/2019 and 2035/2035 is made evident also looking at the spatially averaged AOD daily cycle shown in figures 8 and 9 for the three periods. In addition, huge differences in the shape of the daily cycle in the different considered periods appear.

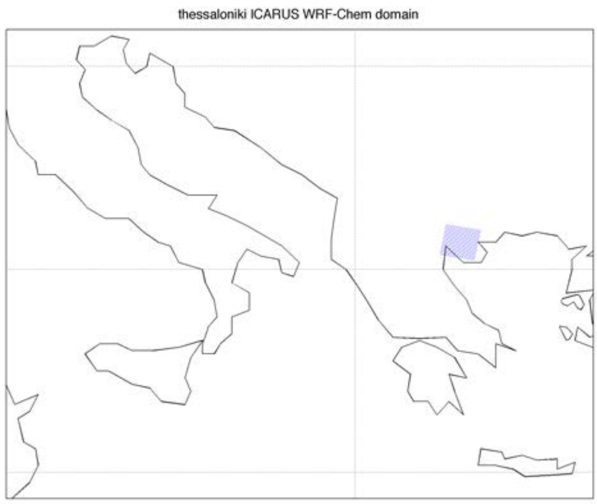

Figure 5: The Thessaloniki WRF-CHEM modeled domain.

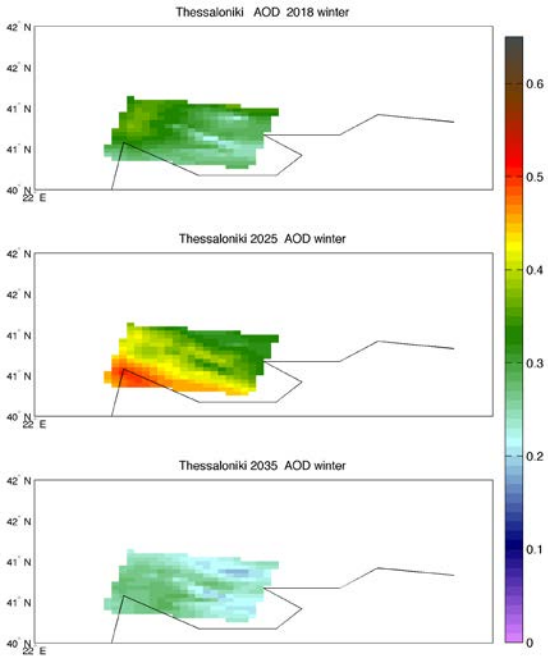

Figure 6: The winter Thessaloniki Aerosol Optical Depth in 2018 2025 and 2035 simulated periods.

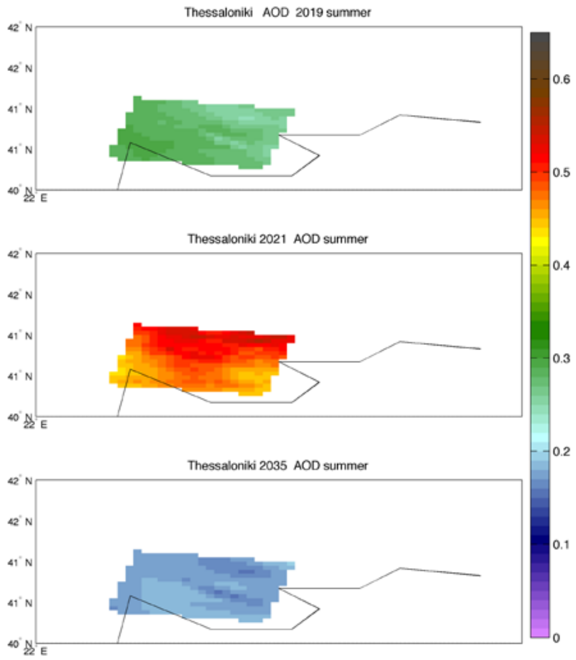

Figure 7: The summer Thessaloniki Aerosol Optical Depth in 2019 2021 and 2035 simulated periods.

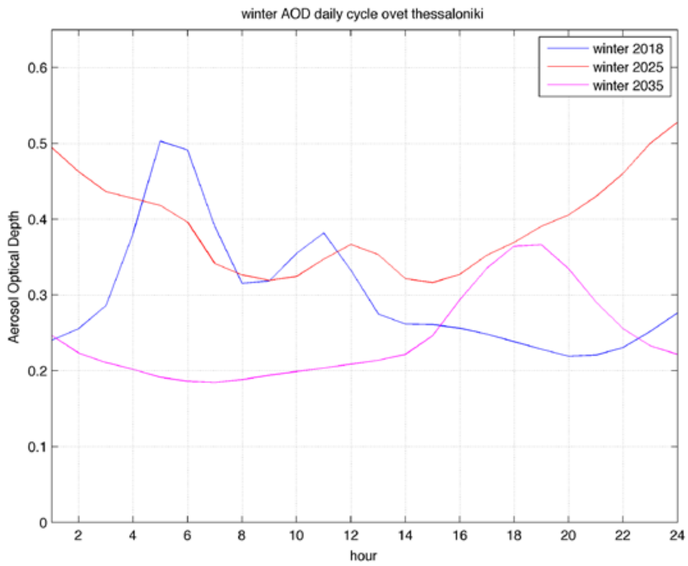

Figure 8: The winter Thessaloniki Aerosol Optical Depth simulated daily cycle in 2018 2025 and 2035.

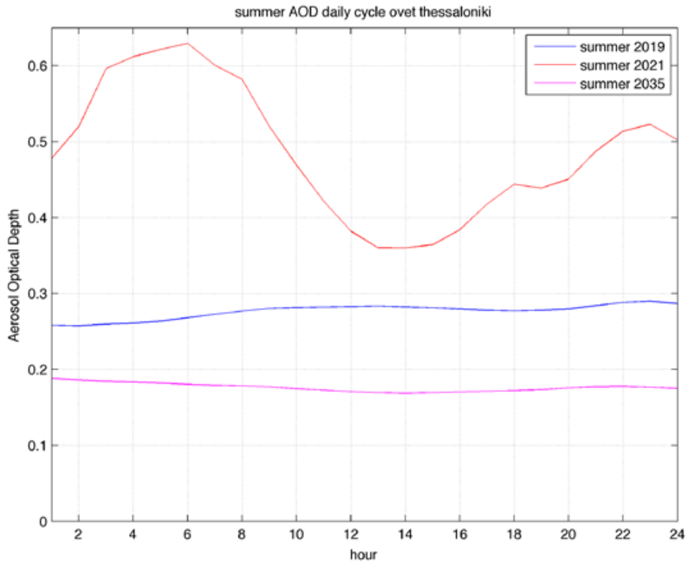

Figure 9: The summer Thessaloniki Aerosol Optical Depth simulated daily cycle in 2019 2021 and 2035.

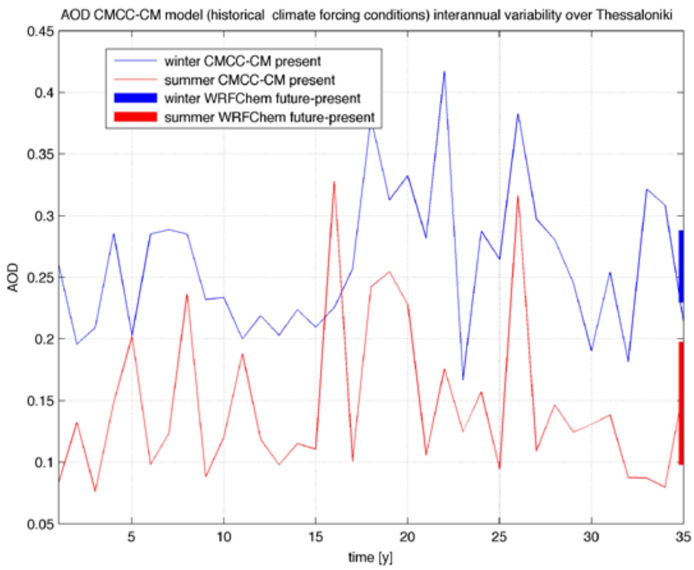

Figure 10: The Thessaloniki Aerosol Optical Depth projected changes (thick lines indicate the amplitude of the projected changes) compared to CMCC-CM time series (thin lines).

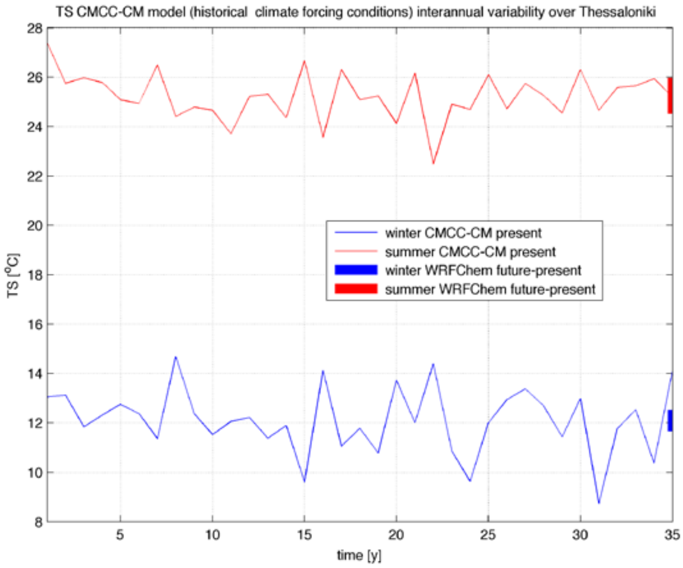

Figure 11: The Thessaloniki Temperature projected changes (thick lines indicate the amplitude of the projected changes) compared to CMCC-CM time series (thin lines).

Figure 10 shows the amplitude of the projected AOD changes in 2035 compared to 2018/2019 for winter/summer (blue/red thick lines) compared to the time series of the CMCC-CM modelled AOD over the same domain and seasons (thin lines). The projected relative ΔF results not statistically significant at the 5% level for both seasons. The projected temperature changes in 2035 with respect to 2018/2019 for winter/summer (blue/red thick lines in figure 11), compared to the time series of the CMCC-CM modelled temperature over the same domain and seasons (thin lines in figure 11), result well confined within the interannual temperature variability over the Thessaloniki domain.

Stuttgart

For the Stuttgart case, differently from what has been shown for the Thessaloniki city, only two periods are available, thus Figures 12 and 13 show the different spatial AOD distribution over the domain, for 2020/2020 and 2035/2034 only, for winter/summer season. Less pronounced differences in AOD are found over Stuttgart, compared to the Thessaloniki case, as also evident in the spatially averaged AOD daily cycle shown in figures 14 and 15 for the two periods. Anyway, during the summer season, the projected changes result more pronounced than what is found for the winter season as also shown by figure 16. The projected relative ΔF results not statistically significant at the 5% level for both seasons, despite the large ΔF found during summer, consistent with the high interannual AOD variability expected over the region (Figure 16).

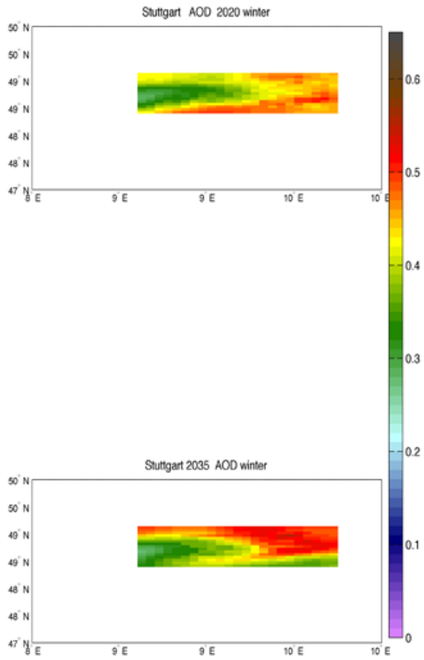

Figure 12: The winter Stuttgart Aerosol Optical Depth in 2020 and 2035 simulated periods.

The projected temperature changes in 2035/2034 with respect to 2020 for winter/summer (blue/red thick lines in figure 17), compared to the time series of the CMCC-CM modelled temperature over the same domain and seasons (thin lines in figure 17), result well confined within the interannual temperature variability over the Stuttgart domain.

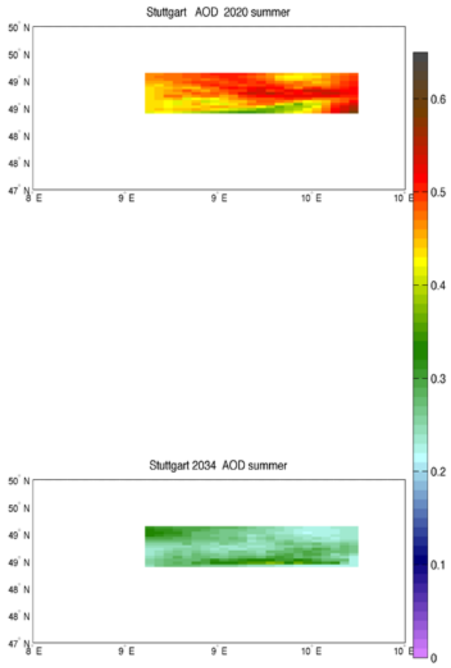

Figure 13: The summer Stuttgart Aerosol Optical Depth in 2020 and 2034 simulated periods.

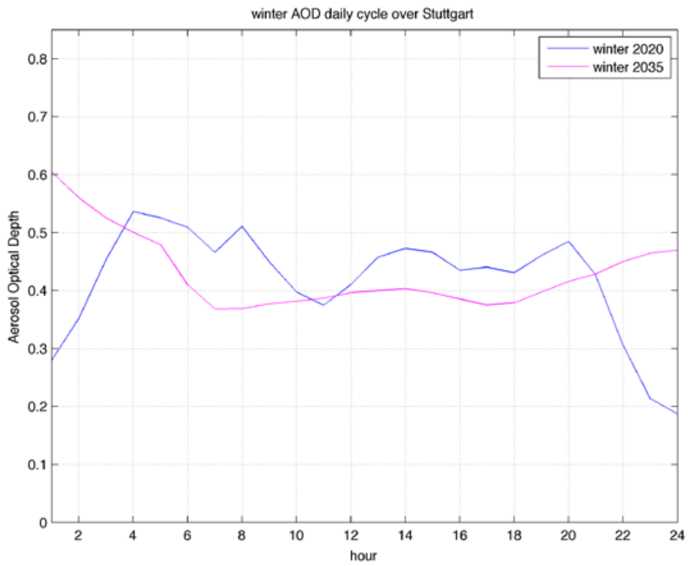

Figure 14: The winter Stuttgart Aerosol Optical Depth simulated daily cycle in 2020 and 2035.

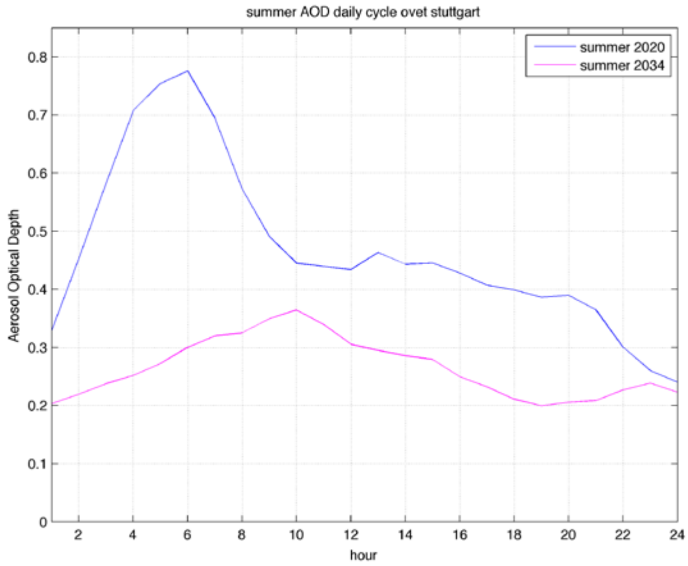

Figure 15: The summer Stuttgart Aerosol Optical Depth simulated daily cycle in 2020 and 2034.

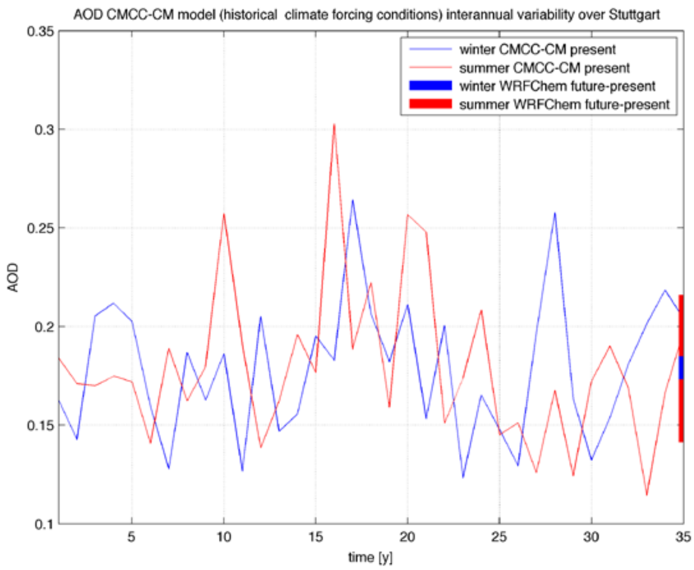

Figure 16: The Stuttgart Aerosol Optical Depth projected changes (thick lines indicate the amplitude of the projected changes) compared to CMCC-CM time series (thin lines).

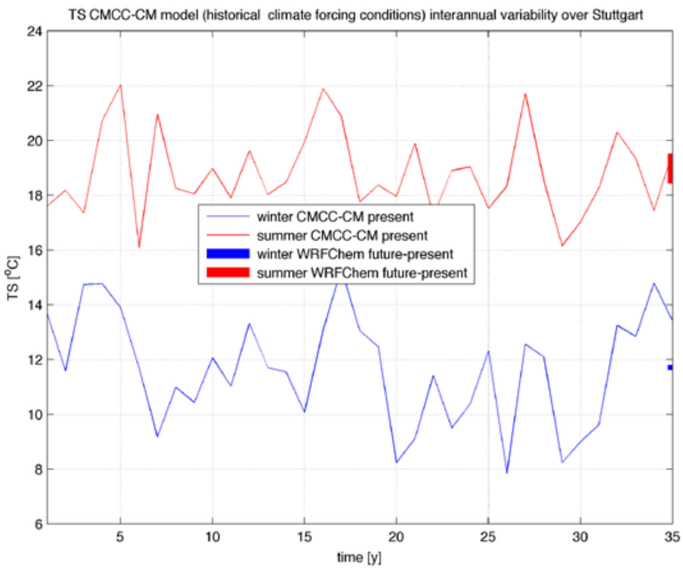

Figure 17: The Stuttgart Temperature projected changes (thick lines indicate the amplitude of the projected changes) compared to CMCC-CM time series (thin lines).

Milan

Differently from Thessaloniki and Stuttgart results, under the two future representative years considered for the Milan city, an increase in AOD is expected during both winter (Figure 18) and summer (Figure 19) with a more pronounced averaged increase expected for the summer season (Figure 21 compared to Figure 20), associated to different spatial AOD differences over the domain. In addition, huge differences in the shape of the daily cycle in the different considered periods appear.

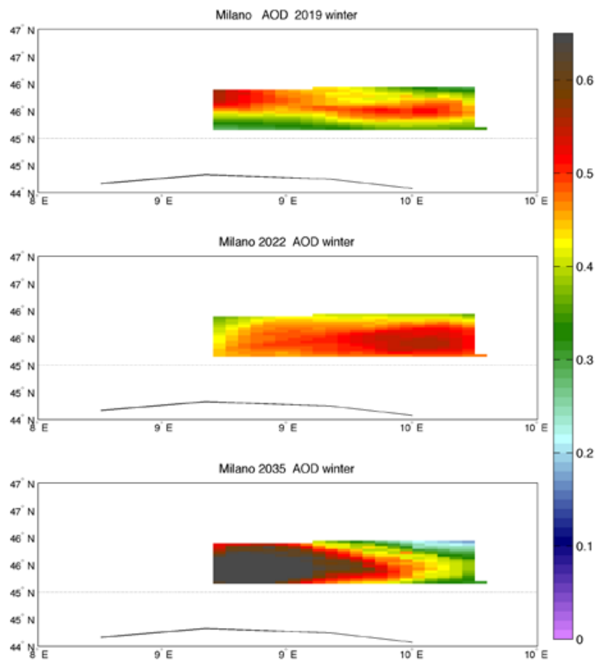

Figure 18: The winter Milan Aerosol Optical Depth in 2018 2025 and 2035 simulated periods.

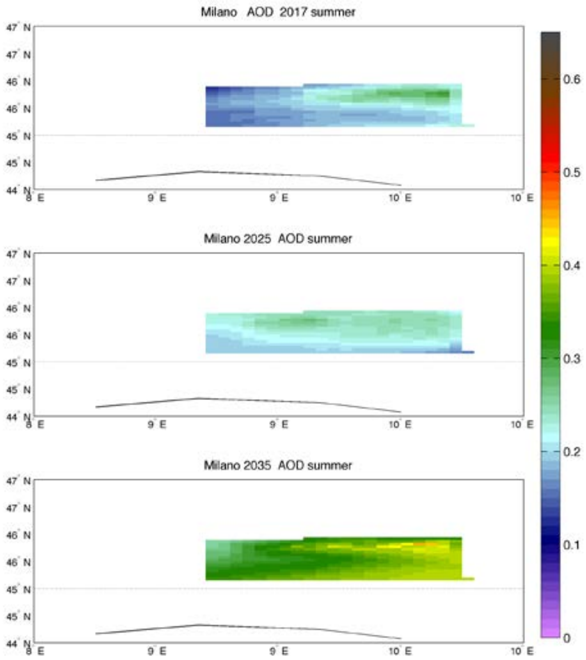

Figure 19: The summer Milan Aerosol Optical Depth in 2019 2021 and 2035 simulated periods.

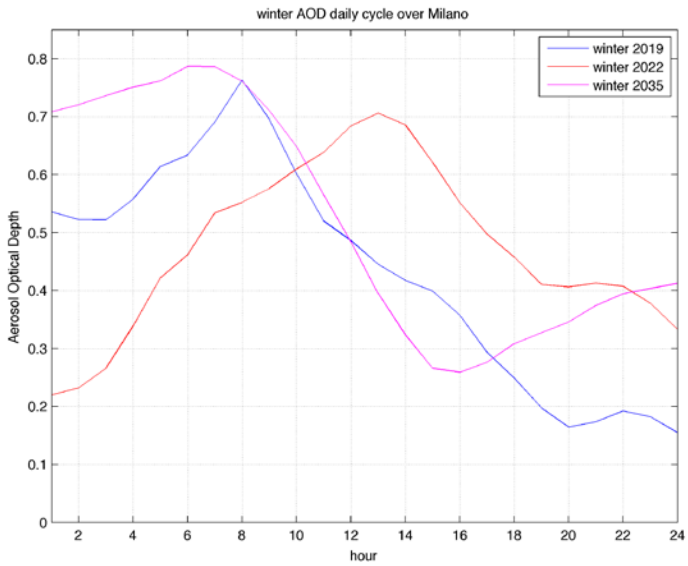

Figure 20: The winter Milan Aerosol Optical Depth simulated daily cycle in 2018 2025 and 2035.

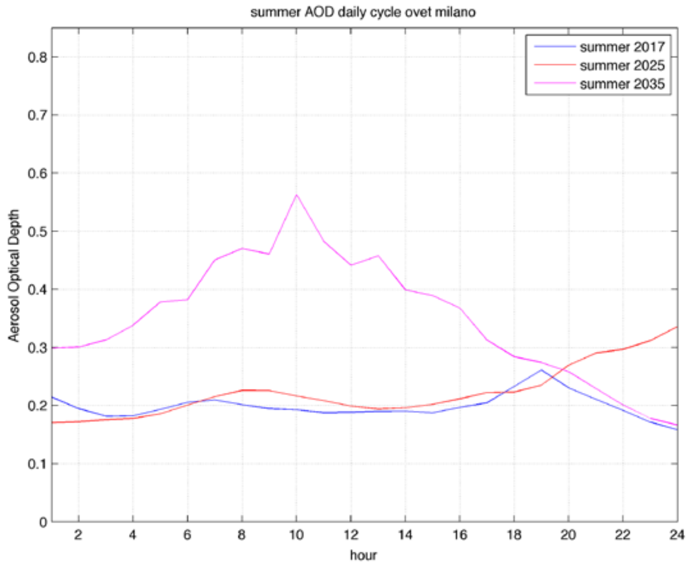

Figure 21: The summer Milan Aerosol Optical Depth simulated daily cycle in 2019 2021 and 2035.

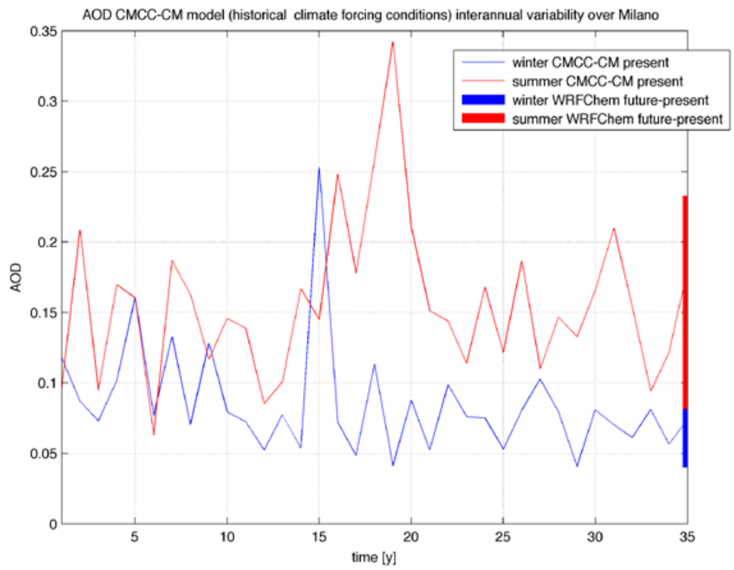

Figure 22: The Milan Aerosol Optical Depth projected changes (thick lines indicate the amplitude of the projected changes) compared to CMCC-CM time series (thin lines).

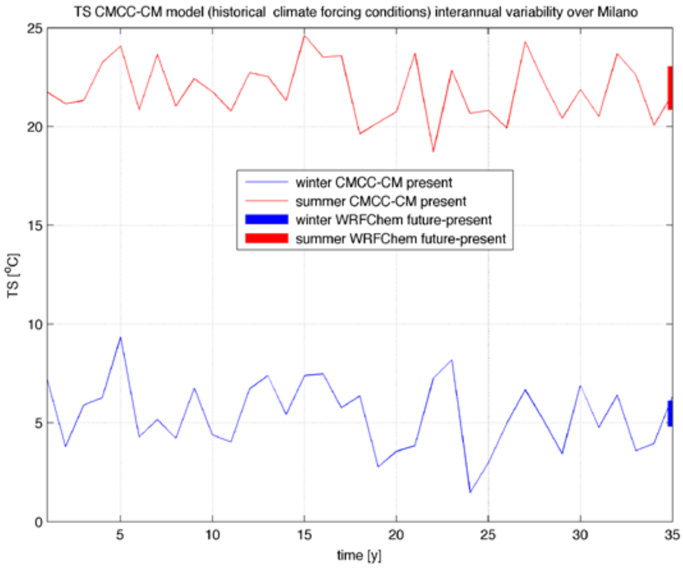

Figure 23: The Milan Temperature projected changes (thick lines indicate the amplitude of the projected changes) compared to CMCC-CM time series (thin lines).

Figure 22 shows the amplitude of the projected AOD changes in 2035 compared to 2018/2019 for winter/summer (blue/red thick lines) compared to the time series of the CMCC-CM modelled AOD over the same domain and seasons (thin lines). Also in this case the projected relative ΔF results not statistically significant at the 5% level for both seasons. The projected temperature changes in 2035 with respect to 2019/2017 for winter/summer (blue/red thick lines in figure 23), compared to the time series of the CMCC-CM modelled temperature over the same domain and seasons (thin lines in figure 23), result well confined within the interannual temperature variability over the Milan domain.

Madrid

Over Madrid small changes are found in AOD during both winter (Figure 24) and summer (Figure 25) with a more pronounced averaged increase expected for the summer season (Figure 26 compared to Figure 27) in the intermediate year only. The daily cycle in the different considered periods appears particularly flat with respect to the other cities considered.

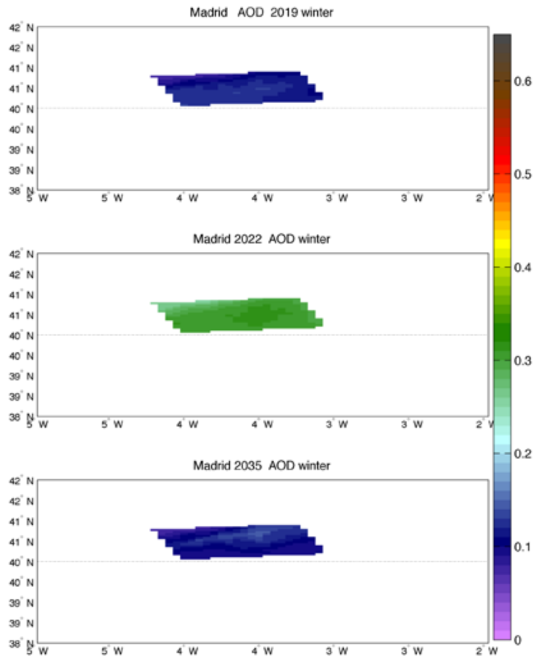

Figure 24: The winter Madrid Aerosol Optical Depth in 2019 2022 and 2035 simulated periods.

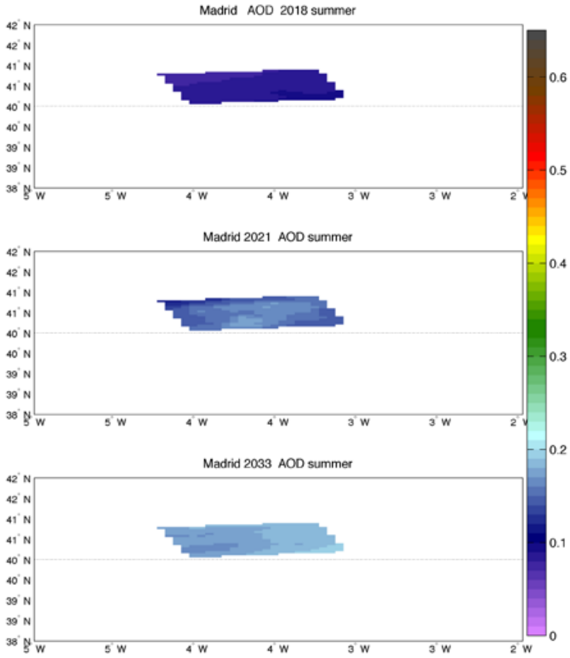

Figure 25: The summer Madrid Aerosol Optical Depth in 2018 2021 and 2033 simulated periods.

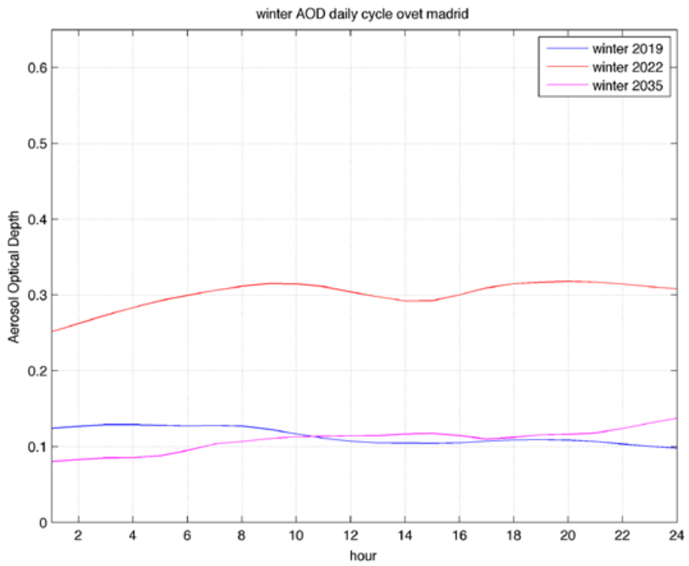

Figure 26: The winter Madrid Aerosol Optical Depth simulated daily cycle in 2019 2022 and 2035.

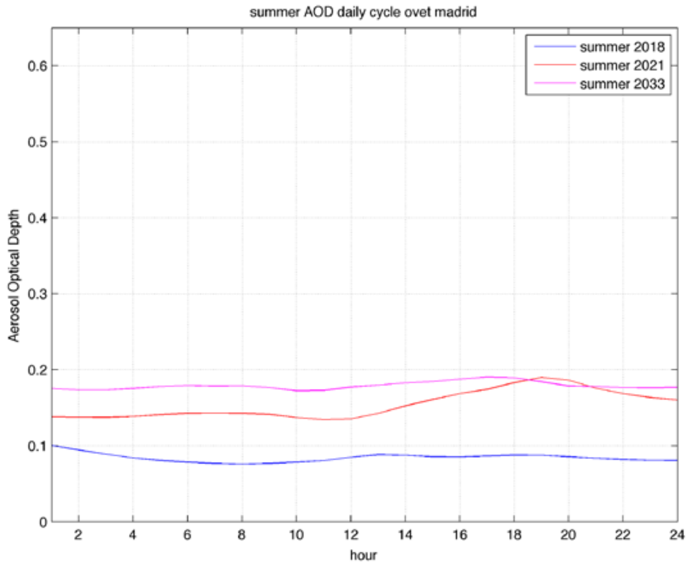

Figure 27: The summer Madrid Aerosol Optical Depth simulated daily cycle in 2018 2021 and 2033.

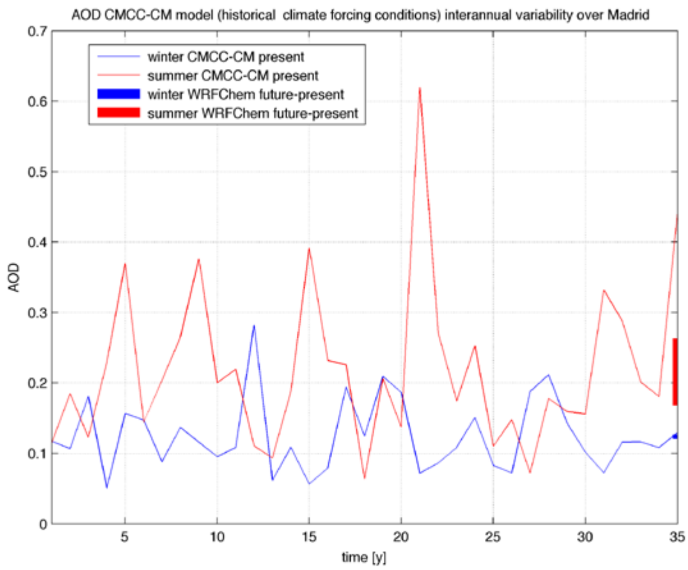

Figure 28: The Madrid Aerosol Optical Depth projected changes (thick lines indicate the amplitude of the projected changes) compared to CMCC-CM time series (thin lines).

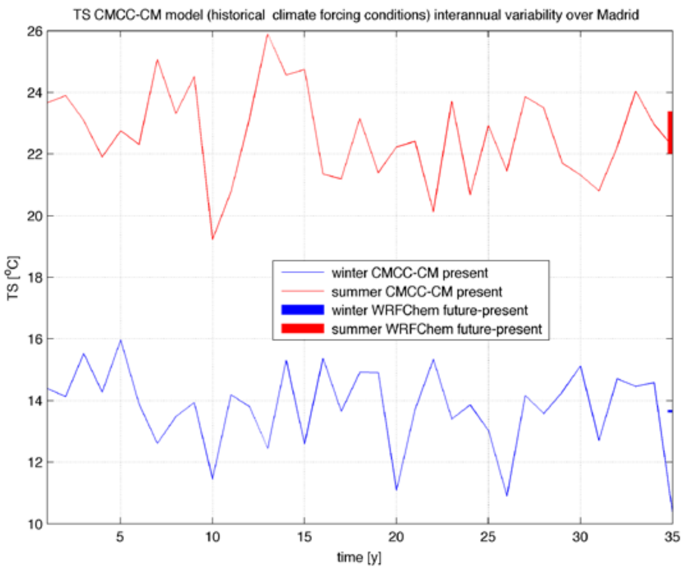

Figure 29: The Madrid Temperature projected changes (thick lines indicate the amplitude of the projected changes) compared to CMCC-CM time series (thin lines).

Figure 28 shows the amplitude of the projected AOD changes in 2035/2033 compared to 2019/2018 for winter/summer (blue/red thick lines) compared to the time series of the CMCC-CM modelled AOD over the same domain and seasons (thin lines). Also in this case the projected relative ΔF results not statistically significant at the 5% level for both seasons. The projected temperature changes in 2035/2033 with respect to 2019/2018 for winter/summer (blue/red thick lines in figure 29), compared to the time series of the CMCC-CM modelled temperature over the same domain and seasons (thin lines in figure 29), result well confined within the interannual temperature variability over the Madrid domain. The more pronounced changes found for the 2022 winter compared to the 2035 results, reinforce the needs for an extension of the period to investigate, in order to have a characterization of the entire internal variability of the climate system.

Ljubljana

Over Ljubljana the most pronounced changes in AOD are found for the late period, during both winter (Figure 30) and summer (Figure 31), in the southeastern part of the domain. Significant changes in the shape of the AOD daily cycle are found during both seasons (Figure 32 compared to Figure 33).

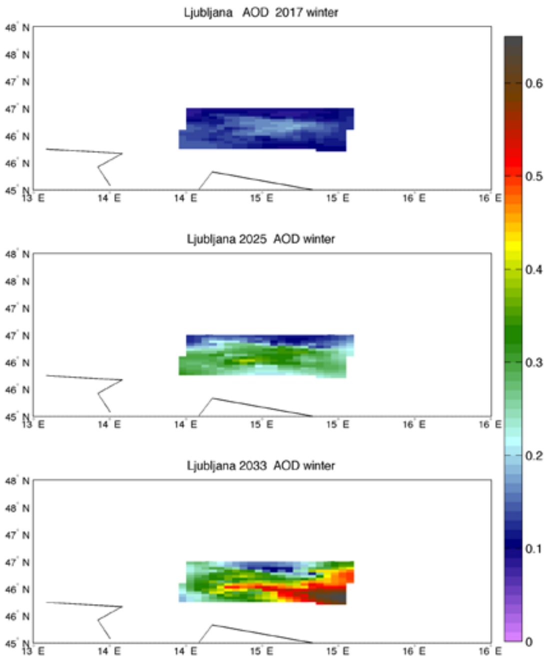

Figure 30: The winter Ljubljana Aerosol Optical Depth in 2017 2025 and 2035 simulated periods.

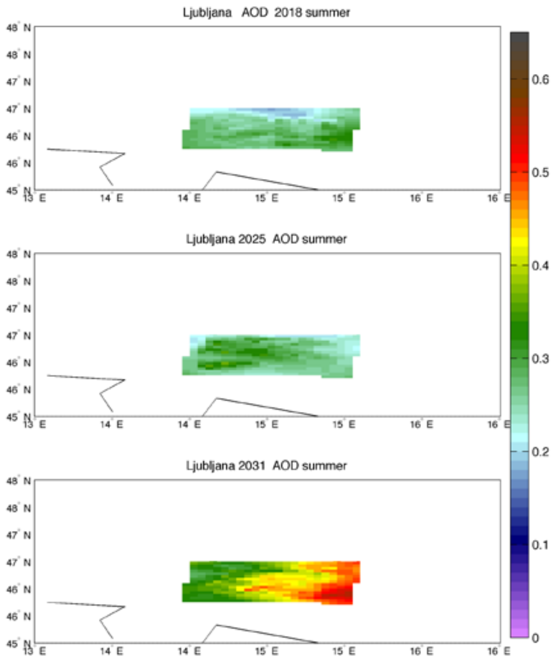

Figure 31: The summer Ljubljana Aerosol Optical Depth in 2018 2025 and 2031 simulated periods.

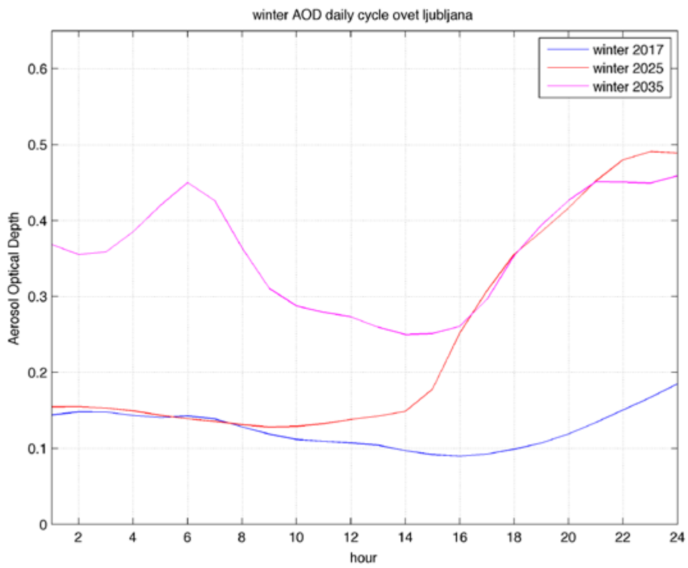

Figure 32: The winter Ljubljana Aerosol Optical Depth simulated daily cycle in 2017 2025 and 2035.

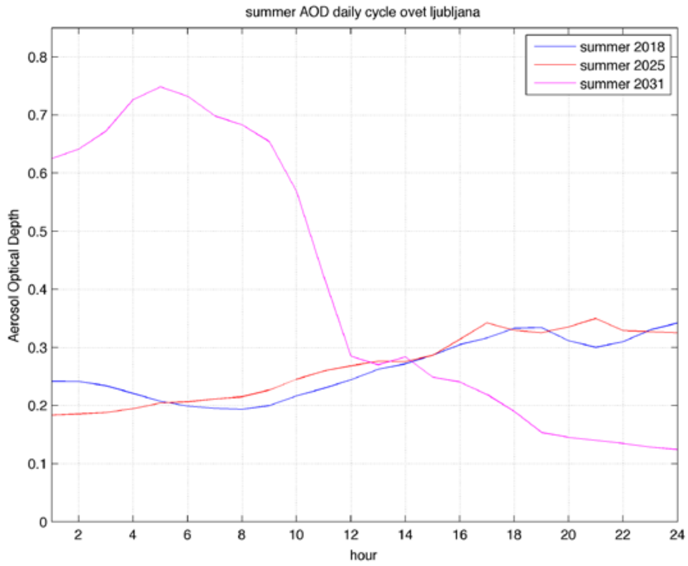

Figure 33: The summer Ljubljana Aerosol Optical Depth simulated daily cycle in 2018 2025 and 2031.

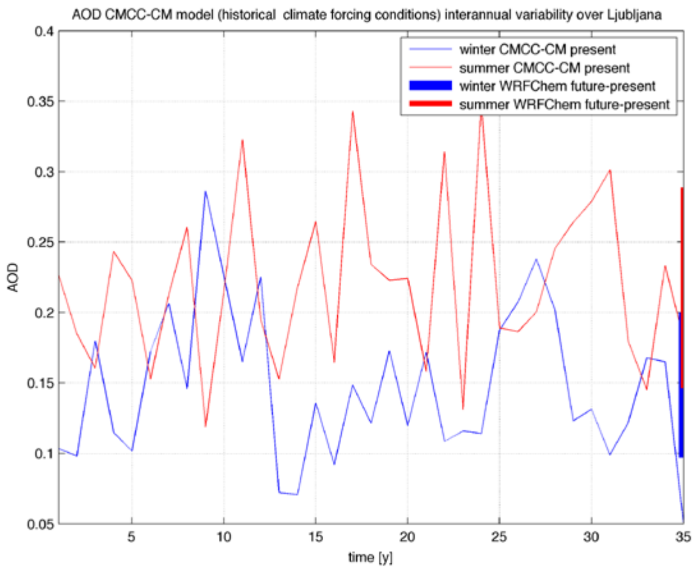

Figure 34: The Ljubljana Aerosol Optical Depth projected changes (thick lines indicate the amplitude of the projected changes) compared to CMCC-CM time series (thin lines).

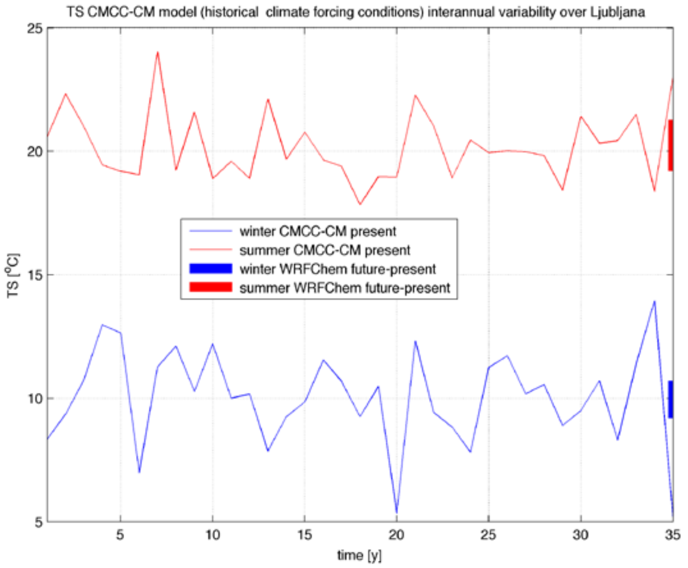

Figure 35: The Ljubljana Temperature projected changes (thick lines indicate the amplitude of the projected changes) compared to CMCC-CM time series (thin lines).

Figure 34 shows the amplitude of the projected AOD changes in 2035/2031 compared to 2018/2017 for winter/summer (blue/red thick lines) compared to the time series of the CMCC-CM modelled AOD over the same domain and seasons (thin lines). Despite the large differences found, the projected relative ΔF results not statistically significant at the 5% level for both seasons, mainly determined by the high interannual variability of the AOD over the considered domain during both seasons (figure 34). The projected temperature changes in 2035/2031 with respect to 2018/2017 for winter/summer (blue/red thick lines in figure 35), compared to the time series of the CMCC-CM modelled temperature over the same domain and seasons (thin lines in figure 35), result well confined within the interannual temperature variability over the Ljubljana domain.

Copenhagen

Over Copenhagen the most pronounced changes in AOD are found for the intermediate period, during both winter (Figure 36) and summer (Figure 37) seasons, with a more pronounced increase found for the winter season. Also in this case significant changes in the shape of the AOD daily cycle are found during both seasons (Figure 38 compared to Figure 39).

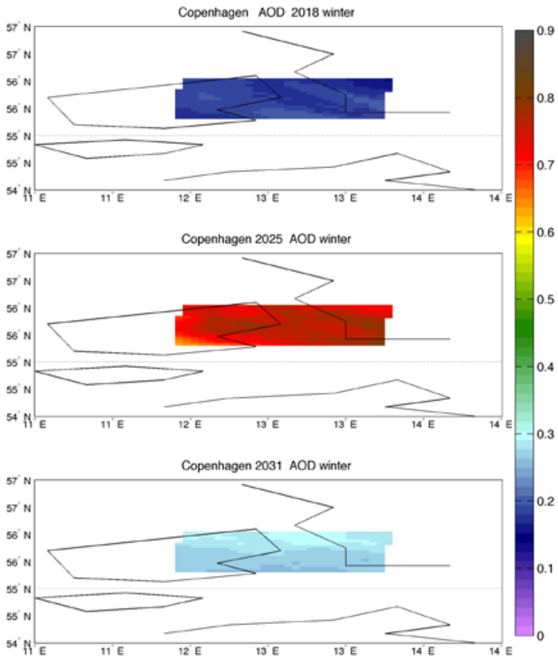

Figure 36: The winter Copenhagen Aerosol Optical Depth in 2018 2025 and 2031 simulated periods.

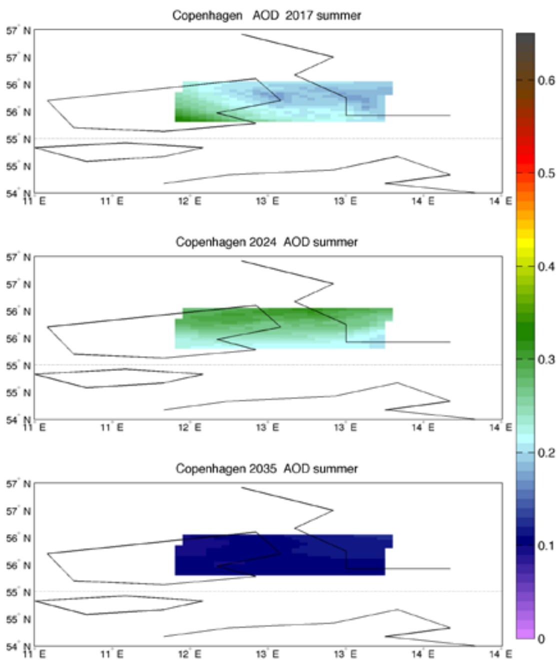

Figure 37: The summer Copenhagen Aerosol Optical Depth in 2017 2024 and 2035 simulated periods.

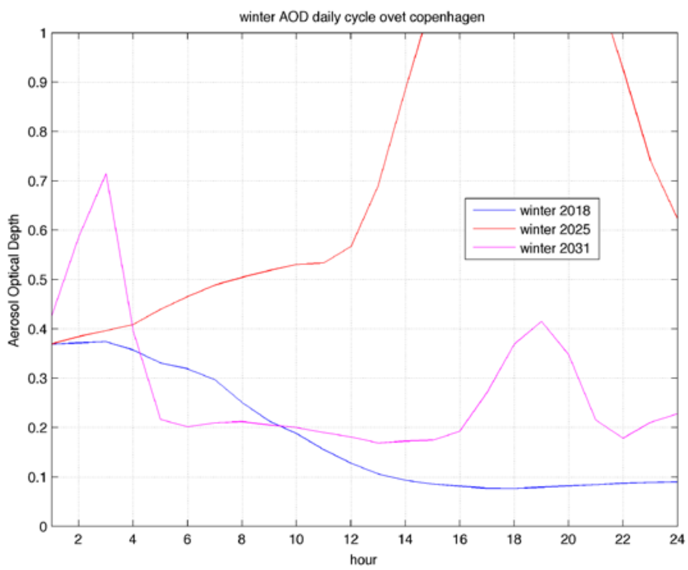

Figure 38: The winter Copenhagen Aerosol Optical Depth simulated daily cycle in 2018 2025 and 2031.

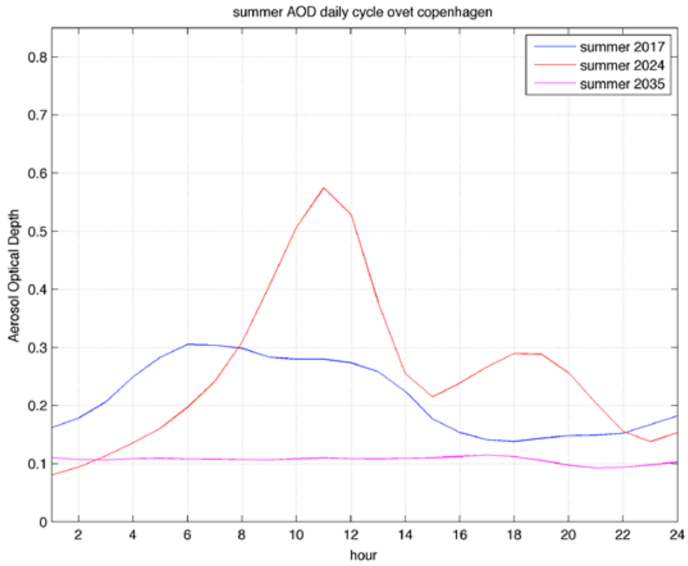

Figure 39: The summer Copenhagen Aerosol Optical Depth simulated daily cycle in 2017 2024 and 2035.

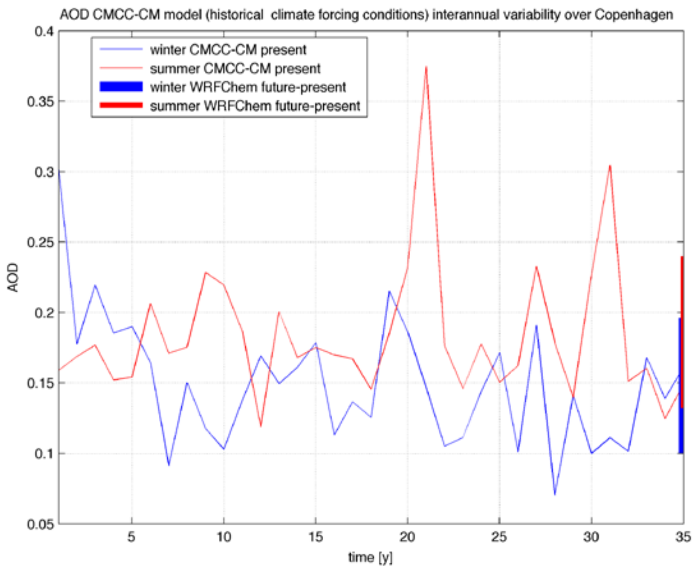

Figure 40: The Copenhagen Aerosol Optical Depth projected changes (thick lines indicate the amplitude of the projected changes) compared to CMCC-CM time series (thin lines).

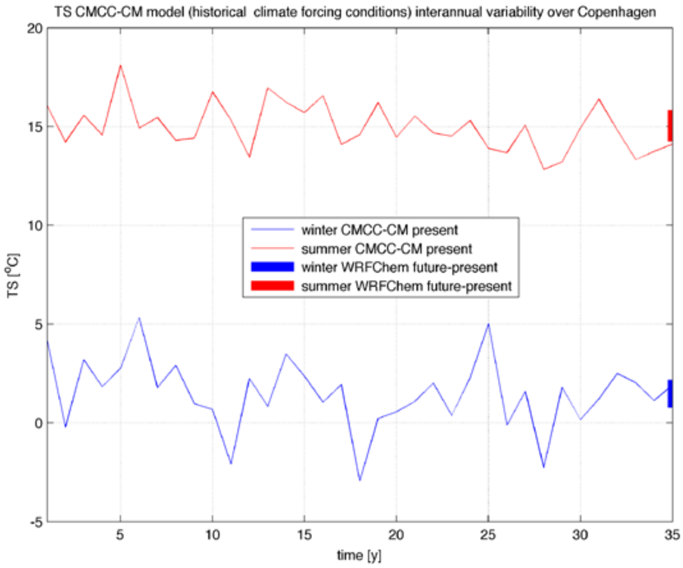

Figure 41: The Copenhagen Temperature projected changes (thick lines indicate the amplitude of the projected changes) compared to CMCC-CM time series (thin lines).

Figure 40 shows the amplitude of the projected AOD changes in 2035/2031 compared to 2018/2017 for winter/summer (blue/red thick lines) compared to the time series of the CMCC-CM modelled AOD over the same domain and seasons (thin lines). The projected relative ΔF results not statistically significant at the 5% level for both seasons (figure 36). The projected temperature changes in 2035/2031 with respect to 2018/2017 for winter/summer (blue/red thick lines in figure 41), compared to the time series of the CMCC-CM modelled temperature over the same domain and seasons (thin lines in figure 41), result well confined within the interannual temperature variability over the Copenhagen domain.

Brno

Over Brno AOD decreases in the intermediate period (2022) during winter and then increases again in 2031, up to values close to the 2019 ones (Figure 42).Again, this might be considered consistent with the interannual variability over the region. A less pronounced oscillation is found for the summer season (Figure 43). Also in this case significant changes in the shape of the AOD daily cycle are found during both seasons (Figure 44 compared to Figure 45).

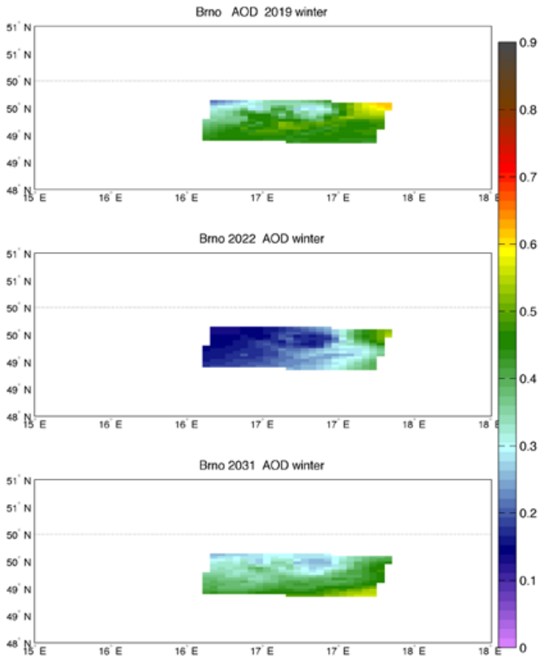

Figure 42: The winter Brno Aerosol Optical Depth in 2019 2022 and 2031 simulated periods.

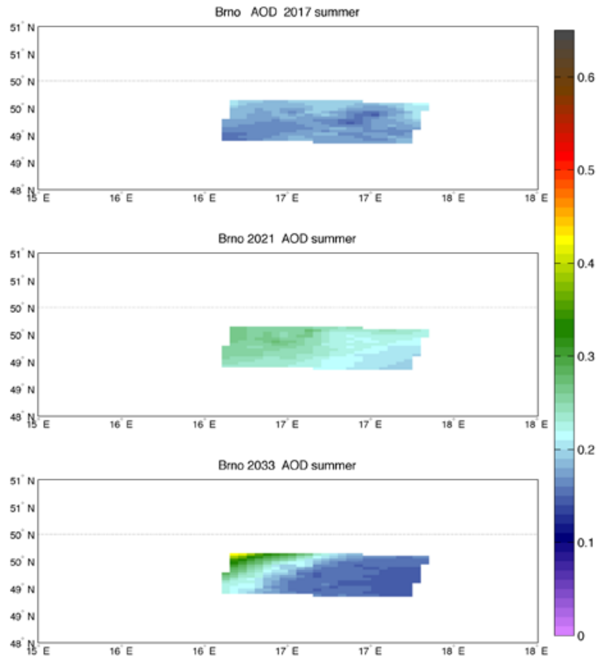

Figure 43: The summer Brno Aerosol Optical Depth in 2017 2021 and 2033 simulated periods.

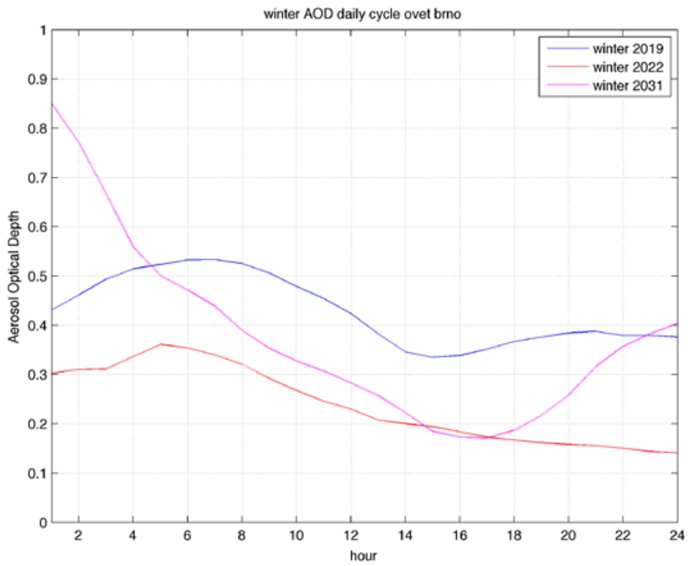

Figure 44: The winter Brno Aerosol Optical Depth simulated daily cycle in 2019 2022 and 2031.

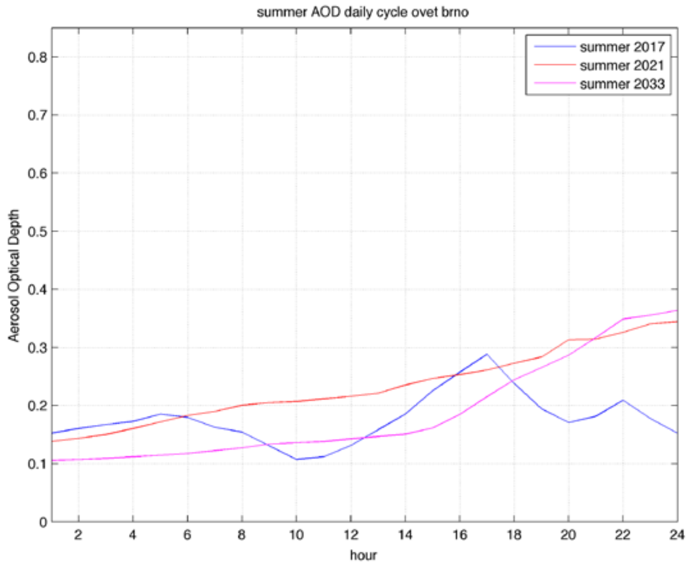

Figure 45: The summer Brno Aerosol Optical Depth simulated daily cycle in 2017 2021 and 2033.

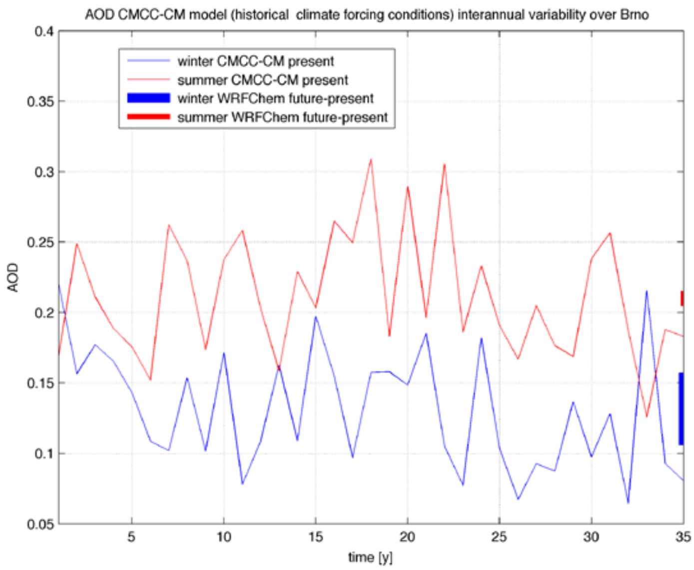

Figure 46: The Brno Aerosol Optical Depth projected changes (thick lines indicate the amplitude of the projected changes) compared to CMCC-CM time series (thin lines).

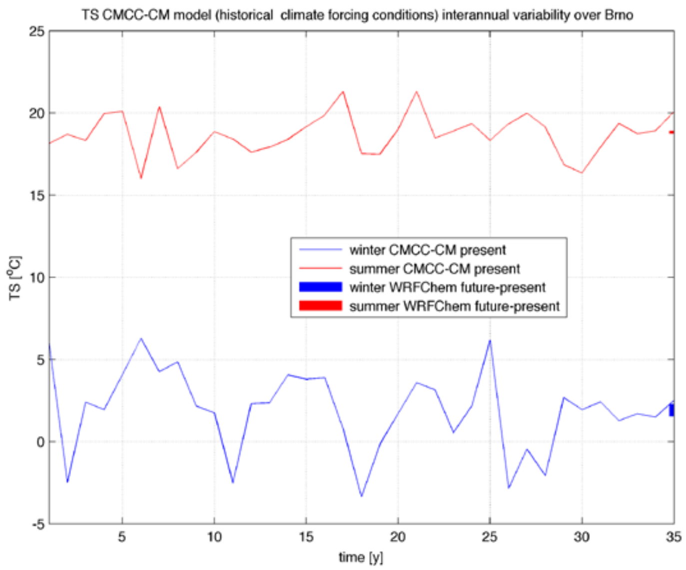

Figure 47: The Brno Temperature projected changes (thick lines indicate the amplitude of the projected changes) compared to CMCC-CM time series (thin lines).

Figure 46 shows the amplitude of the projected AOD changes in 2031/2033 compared to 2019/2017 for winter/summer (blue/red thick lines) compared to the time series of the CMCC-CM modelled AOD over the same domain and seasons (thin lines). The projected relative ΔF results not statistically significant at the 5% level for both seasons (figure 46). The projected temperature changes in 2035/2031 with respect to 2018/2017 for winter/summer (blue/red thick lines in figure 47), compared to the time series of the CMCC-CM modelled temperature over the same domain and seasons (thin lines in figure 47), result well confined within the interannual temperature variability over the Brno domain.

Basel

Also over Basel AOD decreases in the intermediate period (2024) during winter and then increases again in 2035, up to values closer to (but still lower than the 2017 ones (Figure 48)). The opposite is found during summer season when during the intermediate period (2023) the AOD results higher than in 2018 and 2035 (Figure 49). Also in this case significant changes in the shape of the AOD daily cycle are found during both seasons (Figure 50 compared to Figure 51) over the considered domain.

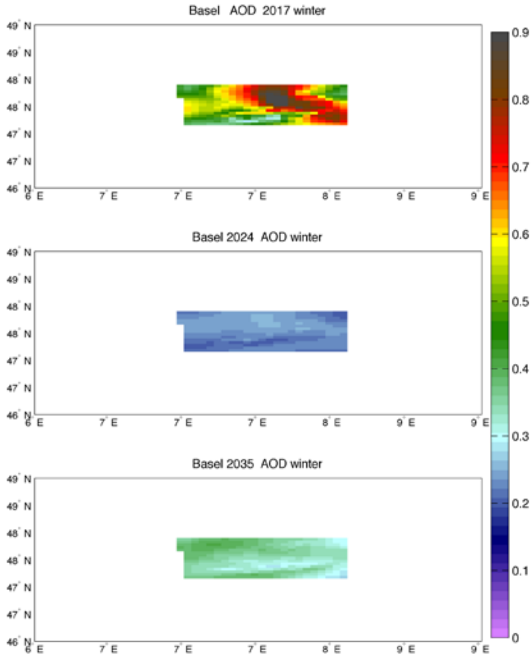

Figure 48: The winter Basel Aerosol Optical Depth in 2017 2024 and 2035 simulated periods.

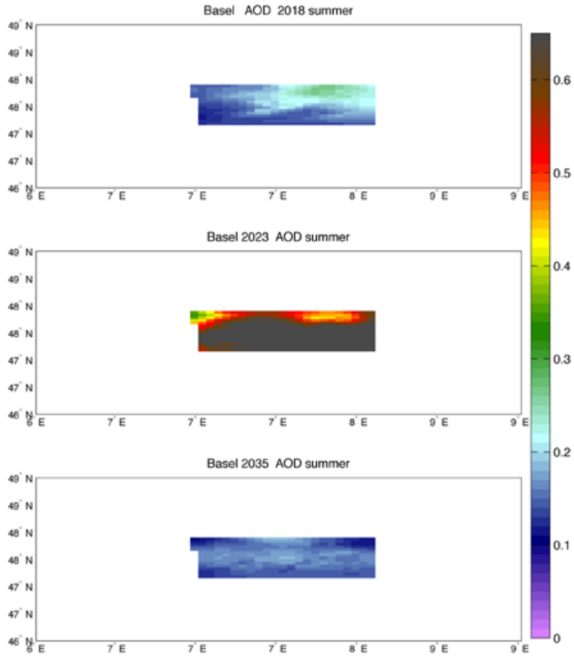

Figure 49: The summer Basel Aerosol Optical Depth in 2018 2023 and 2035 simulated periods.

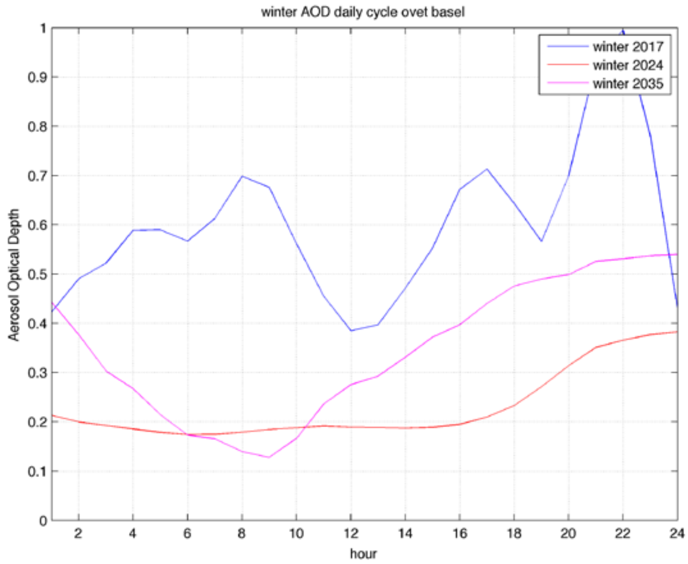

Figure 50: The winter Basel Aerosol Optical Depth simulated daily cycle in 2017 2024 and 2035.

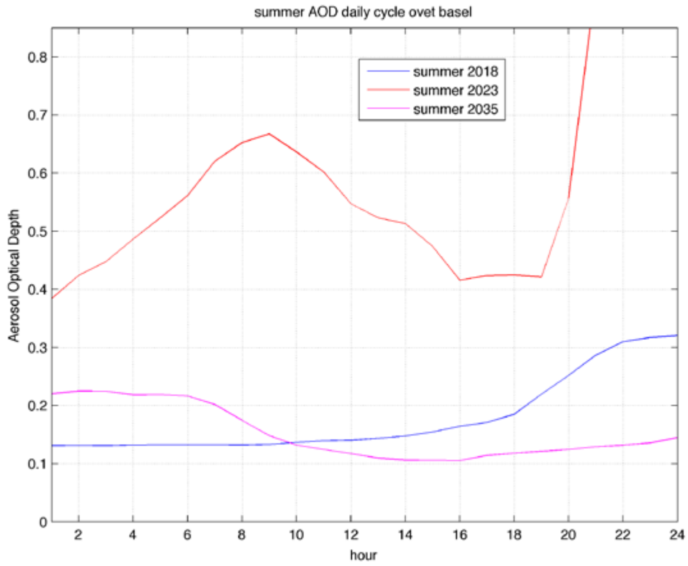

Figure 51: The summer Basel Aerosol Optical Depth simulated daily cycle in 2017 2021 and 2033.

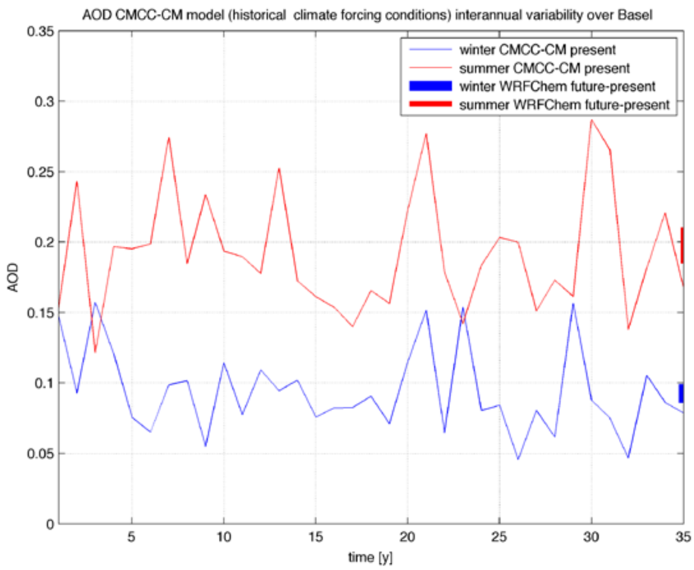

Figure 52: The Basel Aerosol Optical Depth projected changes (thick lines indicate the amplitude of the projected changes) compared to CMCC-CM time series (thin lines).

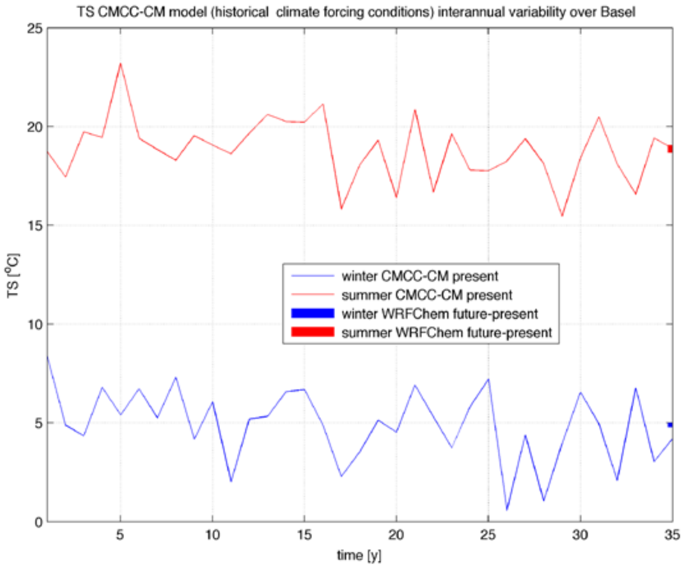

Figure 53: The Basel Temperature projected changes (thick lines indicate the amplitude of the projected changes) compared to CMCC-CM time series (thin lines).

Figure 51 shows the amplitude of the projected AOD changes in 2035 compared to 2017/2018 for winter/summer (blue/red thick lines) compared to the time series of the CMCC-CM modelled AOD over the same domain and seasons (thin lines). The projected relative ΔF results not statistically significant at the 5% level for both seasons (figure 52). The projected temperature changes in 2035 with respect to 2017/2018 for winter/summer (blue/red thick lines in figure 53), compared to the time series of the CMCC-CM modelled temperature over the same domain and seasons (thin lines in figure 53), result well confined within the interannual temperature variability over the Basel domain.

Athens

Over Athens, AOD decreases in 2033 compared to 2019 values, with a more pronounced change during the summer season (Figure 54 and Figure 55). The shape of the daily cycle remains almost flat in the three considered years during winter (figure 56), but significant changes in the shape of the AOD daily cycle are found during summer (Figure 57) over the considered domain.

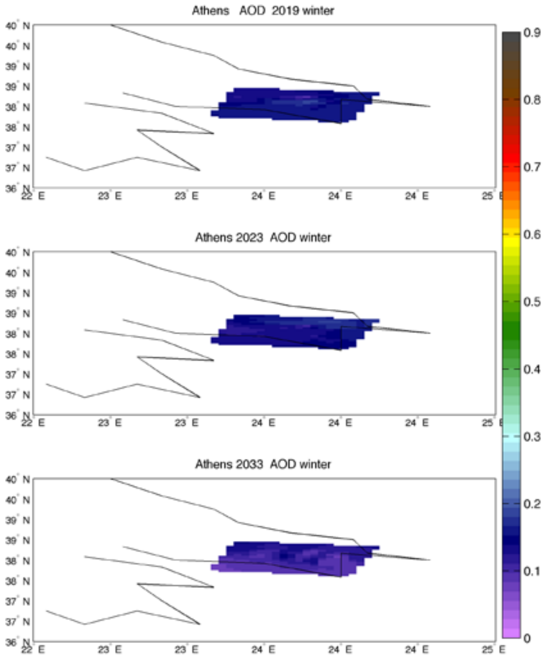

Figure 54: The winter Athens Aerosol Optical Depth in 2019 2023 and 2033 simulated periods.

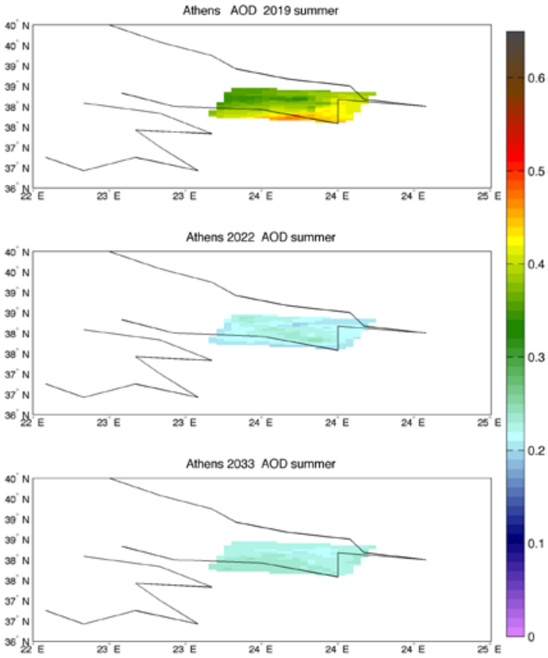

Figure 55: The summer Athens Aerosol Optical Depth in 2019 2022 and 2033 simulated periods.

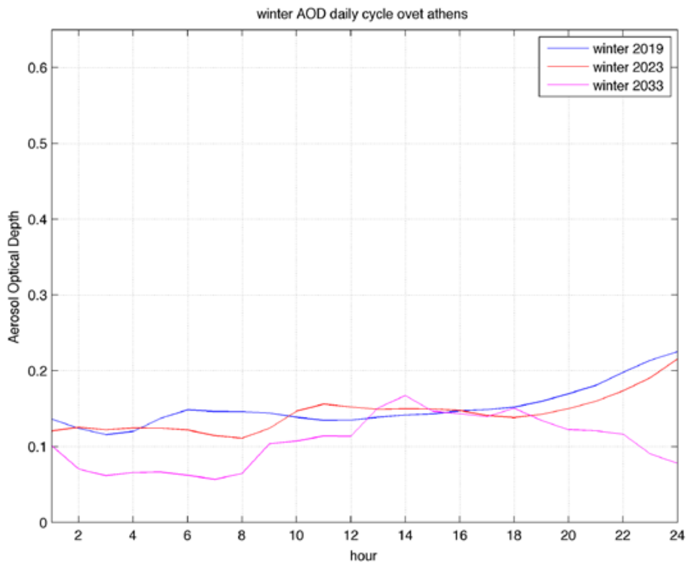

Figure 56: The winter Athens Aerosol Optical Depth simulated daily cycle in 2019 2023 and 2033.

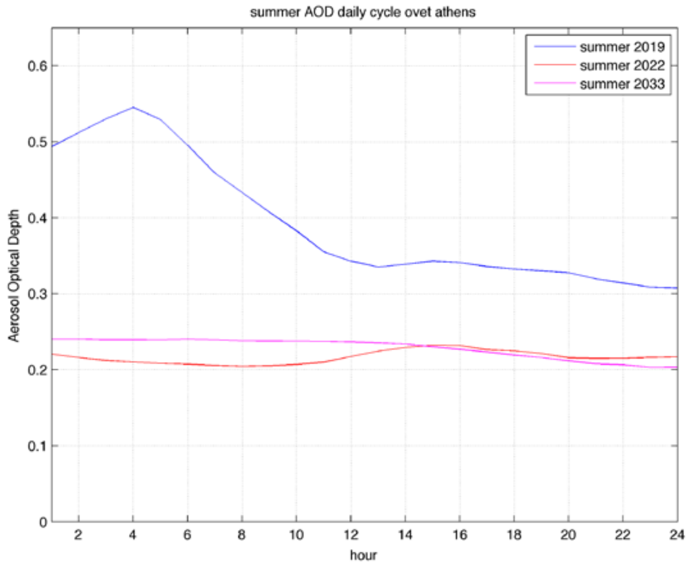

Figure 57: The summer Athens Aerosol Optical Depth simulated daily cycle in 2019 2022 and 2033.

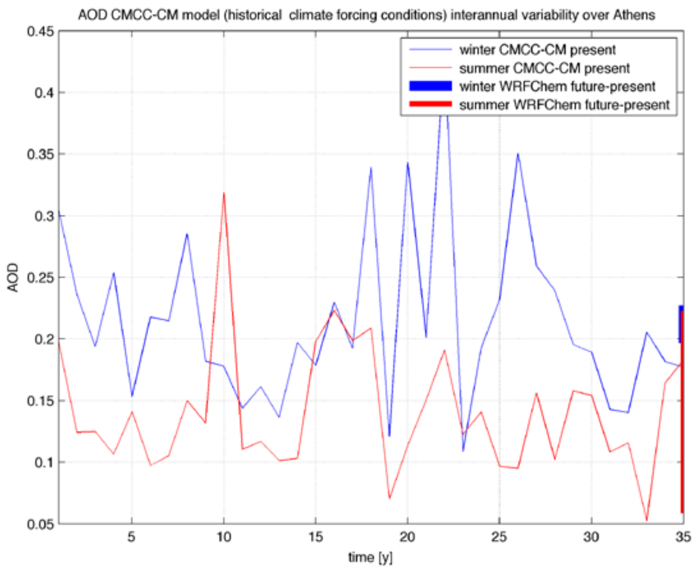

Figure 58 The Athens Aerosol Optical Depth projected changes (thick lines indicate the amplitude of the projected changes) compared to CMCC-CM time series (thin lines).

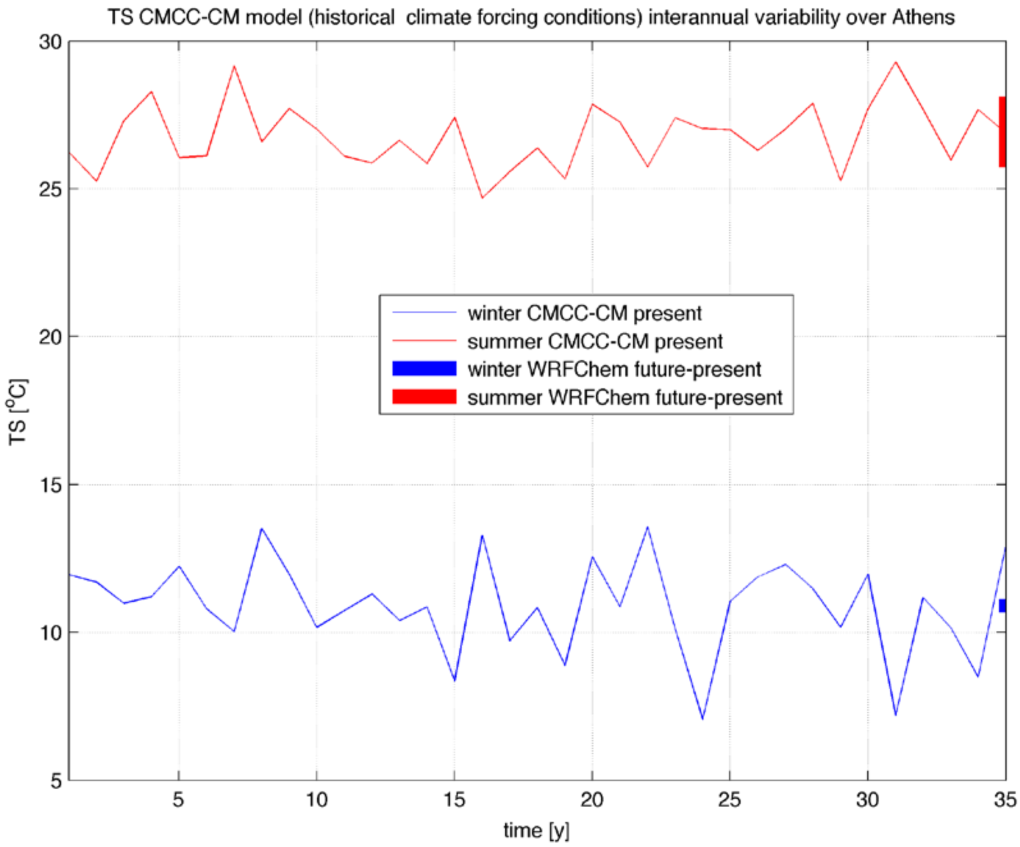

Figure 59: The Athens Temperature projected changes (thick lines indicate the amplitude of the projected changes) compared to CMCC-CM time series (thin lines).

Figure 58 shows the amplitude of the projected AOD changes in 2033 compared to 2019 for winter/summer (blue/red thick lines) compared to the time series of the CMCC-CM modelled AOD over the same domain and seasons (thin lines). The projected relative ΔF results not statistically significant at the 5% level for both seasons (figure 58). The projected temperature changes in 2033 with respect to 2019 for winter/summer (blue/red thick lines in figure 59), compared to the time series of the CMCC-CM modelled temperature over the same domain and seasons (thin lines in figure 59), result well confined within the interannual temperature variability over the Athens domain despite the projected changes are not negligible during summer.

6 Summary

With the aim to evaluate the changes in the surface radiative forcing associated to the aerosols concentration modification induced by the implementation of mitigation strategies at local level, high resolution regional climate model results (up to 2 km as horizontal resolution) provided within ICARUS have been investigated.
Based on the clustering analysis described in D3.3, the WRF-Chem model has been run at 2 km resolution over the nine ICARUS cities under different climate forcing conditions, following different aerosols emissions resulting from different mitigation approaches.
The characterization of aerosol in terms of global warming potential has been done applying a simplified scheme translating different types of Aerosols Optical Depth changes into a first order assessment of radiative forcing following the Chylek and Henderson (2003) method.
In addition, based on results from a CMCC present climate simulation at the global scale - having an aerosol module implemented within its atmospheric component, we verified the consistency between changes in integrated aerosols concentrations and the relative changes in AOD, associated to mitigation strategies.

For all of the ICARUS cities (Thessaloniki, Stuttgart, Milano, Madrid, Ljubjana, Copenaghen, Brno, Basel, Athens) a comparison between radiative forcing associated to future (about 2035) and present (about 2018) periods has been done, in terms of AOD differences and temperature induced changes after the application of ICARUS mitigation strategies. Also an intermediate period (between 2018 and 2035) is investigated to provide additional information in terms of internnual variability. The ΔF estimate between future and past is computed and its significance is evaluated based on a Montecarlo approach at the 5% level building on of the series of numbers provided by the CMCC-CM model over the 35y period considered. The results for each cities are presented not only in terms of AOD changes but also in terms of estimated induced temperature changes.

No significant differences in terms of radiative forcing have been found over all of the ICARUS cities between the past and future period considered and the induced changes in temperature well remain within the interannual variability of the region. Anyway, the short period simulated (due to computational limitations) around each considered date may be not sufficient to realistically represent climate conditions over the region: a longer period would be necessary to give significance to the repesentativeness of the presented results.

For the aforementioned reasons, this document only provides a metodological approach to perform the required analysis on the impact on the local climate induced by mitigation strategies in terms of aerosols emission reduction.

7 References

Cagnazzo, C., E. Manzini, M. A. Giorgetta, P. M. F. Forster, and J. J. Morcrette (2007), Impact of an improved shortwave radiation scheme in the MAECHAM5 general circulation model, Atmos. Chem. Phys., 7, 2503–2515.

Chylek, P., B. Henderson, and M. Mishchenko, (2003), Aerosol radiative forcing and the accuracy of satellite aerosol optical depth retrieval. *J. Geophys. Res.*, **108**, no. D24, 4764, doi:10.1029/2003JD004044.

D'Errico, M., C. Cagnazzo, P. G. Fogli, W. K. M. Lau, J. von Hardenberg, F. Fierli, and A. Cherchi (2015), Indian monsoon and the elevated-heat-pump mechanism in a coupled aerosol-climate model, J. Geophys. Res. Atmos., 120, 8712–8723,doi:10.1002/2015JD023346.

Dentener, F., et al. (2006), Emissions of primary aerosol and precursor gases in the years 2000 and 1750, prescribed data-sets for AeroCom, Atmos. Chem. Phys. Discuss., 6, 2703–2763.

Doms G. and J Förstner (2004). Developmentof a kilometerscalenwpsystem: Lmk. COSMO Newsletter , 4:159–167.

Fogli, P. G., et al. (2009), INGV-CMCC carbon: A carbon cycle Earth system model, CMCC online RP0061. [Available at http://www.cmcc.it/publications-meetings/publications/research-papers/rp0061-ingvcmcc-carbon-icc-a-carbon-cycle-earth-system-model.

Folini, D., and M. Wild (2011), Aerosol emissions and dimming/brightening in Europe: Sensitivity studies with ECHAM5-HAM, J. Geophys. Res., 116, D21104, doi:10.1029/2011JD016227.

Henriksson, S. V., A. Laaksonen, V. M. Kerminen, P. Räisänen, P. H. Järvinen, A.-M. Sundström, and G. de Leeuw (2011), Spatial distributions and seasonal cycles of aerosols in India and China seen in global climate-aerosol model, Atmos. Chem. Phys., 11, 7975–7990,doi:10.5194/acp-11-7975-2011.

Holton J.R. and Gregory J Hakim. An introduction to dynamic meteorology . Academic press, 2013

Madec, G., P. Delecluse, I. Imbard, and C. Levy (1999), OPA 8.1 ocean general circulation model reference manual, Note du Pôle demodélisation No. 11, Inst. Pierre-Simon Laplace (IPSL), France, 91 pp.

Oddo P. , M Adani, N Pinardi, C Fratianni, M Tonani, and D Pettenuzzo (2009). A nested atlantic mediterranean sea general circulation model for operational forecasting. Ocean science .

Rockel, B., Geyer, B. 2008 The performance of the regional climate model CLM in different climate regions, based on the example of precipitation, Meteorologische Zeitschrift, Vol. 17 (4): 487-498.

Scoccimarro, E., S. Gualdi, A. Bellucci, A. Sanna, P. G. Fogli, E. Manzini, M. Vichi, P. Oddo, and A. Navarra (2011), Effects of tropical cyclones on ocean heat transport in a high resolution coupled general circulation model, J. Clim., 24, 4368–4384.

Schulz, M., G. de Leeuw, and Y. Balkanski (2004), Sea-salt aerosol source functions and emissions, in Emission of Atmospheric Trace Compounds, edited by C. Granier, P. Artaxo, and C. E. Reeves, pp. 333–359, Kluwer Acad., Dordrecht, Netherlands.

Stier, P., et al. (2005), The aerosol-climate model ECHAM5-HAM, Atmos. Chem. Phys., 5, 1125–1156.

Stier, P., J. H. Seinfeld, S. Kinne, and O. Boucher (2007), Aerosol absorption and radiative forcing, Atmos. Chem. Phys., 7, 5237–5261, doi:10.5194/acp-7-5237-2007.

J Steppeler, G Doms, U Schättler, HW Bitzer, A Gassmann, U Damrath, and G Gregoric (2003) Meso-gamma scale forecasts using the nonhydrostatic model lm. Me- teorology and atmospheric Physics , 82(14): 75–96.

Tiedtke M. (1989). A comprehensive mass flux scheme for cumulus parameterization in largescale models. Monthly Weather Review , 117(8):1779– 1800.

Tegen, I., S. P. Harrison, K. Kohfeld, I. C. Prentice, M. Coe, and M. Heimann (2002), Impact of vegetation and preferential source areas on global dust aerosols: Results from a model study, J. Geophys. Res., 107(D21), 4576, doi:10.1029/2001JD000963.

Tegen, I., M. Werner, S. P. Harrison, and K. E. Kohfeld (2004), Relative importance of climate and land use in determining present and future global soil dust emission, Geophys. Res. Lett., 31, L05105, doi:10.1029/2003GL019216.

Van Der Werf, G. R., et al. (2003), Carbon emissions from fires in tropical and subtropical ecosystems, Global Change Biol., 9(4), 547–562.

APPENDIX 1 list of available Aerosols fields

BURDEN_SO4:long_name = "column burden SO4" ;

BURDEN_SO2:long_name = "column burden SO2" ;

BURDEN_DMS:long_name = "column burden DMS" ;

BURDEN_SO4_GAS:long_name = "column burden SO4 gas" ;

BURDEN_BC:long_name = "column burden BC" ;

BURDEN_OC:long_name = "column burden OC" ;

BURDEN_SS:long_name = "column burden SS" ;

BURDEN_DU:long_name = "column burden DU" ;

BURDEN_WAT:long_name = "column burden WAT" ;

BURDEN_NUM:long_name = "column burden NUM" ;

DRY_SO2:long_name = "dry deposition flux SO2" ;

DRY_SO4_GAS:long_name = "dry deposition flux SO4gas " ;

DRY_SO4:long_name = "dry deposition flux SO4" ;

DRY_BC:long_name = "dry deposition flux BC" ;

DRY_OC:long_name = "dry deposition flux OC" ;

DRY_SS:long_name = "dry deposition flux SS" ;

DRY_DU:long_name = "dry deposition flux DU" ;

DRY_NUM:long_name = "dry deposition flux NUM" ;

VDRY_NS:long_name = "dry deposition velocity nucleation mode soluble" ;

VDRY_KS:long_name = "dry deposition velocity Aitken mode soluble" ;

VDRY_AS:long_name = "dry deposition velocity accumulation mode soluble" ;

VDRY_CS:long_name = "dry deposition velocity coarse mode soluble" ;

VDRY_KI:long_name = "dry deposition velocity Aitken mode insoluble" ;

VDRY_AI:long_name = "dry deposition velocity accumulation mode insoluble" ;

VDRY_CI:long_name = "dry deposition velocity coarse mode soluble" ;

WET_SO2:long_name = "wet deposition flux SO2" ;

WET_SO4_GAS:long_name = "wet deposition flux SO4 gas" ;

WET_SO4:long_name = "wet deposition flux SO4" ;

WET_BC:long_name = "wet deposition flux BC" ;

WET_OC:long_name = "wet deposition flux OC" ;

WET_SS:long_name = "wet deposition flux SS" ;

WET_DU:long_name = "wet deposition flux DU" ;

WET_NUM:long_name = "wet deposition flux NUM" ;

WET_CONV_SO2:long_name = "wet deposition flux SO2" ;

WET_CONV_SO4:long_name = "wet deposition flux SO4" ;

WET_CONV_BC:long_name = "wet deposition flux BC" ;

WET_CONV_OC:long_name = "wet deposition flux OC" ;

WET_CONV_SS:long_name = "wet deposition flux SS" ;

WET_CONV_DU:long_name = "wet deposition flux DU" ;

WET_CONV_NUM:long_name = "wet deposition flux NUM" ;

WET_STRAT_SO2:long_name = "wet deposition flux SO2" ;

WET_STRAT_SO4:long_name = "wet deposition flux SO4" ;

WET_STRAT_BC:long_name = "wet deposition flux BC" ;

WET_STRAT_OC:long_name = "wet deposition flux OC" ;

WET_STRAT_SS:long_name = "wet deposition flux SS" ;

WET_STRAT_DU:long_name = "wet deposition flux DU" ;

WET_STRAT_NUM:long_name = "wet deposition flux NUM" ;

SED_SO4:long_name = "sedimentation flux SO4" ;

SED_BC:long_name = "sedimentation flux BC" ;

SED_OC:long_name = "sedimentation flux OC" ;

SED_SS:long_name = "sedimentation flux SS" ;

SED_DU:long_name = "sedimentation flux DU" ;

SED_NUM:long_name = "sedimentation flux NUM" ;

VSED_AS:long_name = "sedimentation velocity accumulation mode soluble" ;

VSED_CS:long_name = "sedimentation velocity coarse mode soluble" ;

VSED_AI:long_name = "sedimentation velocity accumulation mode insoluble" ;

VSED_CI:long_name = "sedimentation velocity coarse mode soluble" ;

EMI_S:long_name = "Emission of S TOTAL" ;

EMI_S_ANT:long_name = "Emission of S ANT" ;

EMI_S_NAT:long_name = "Emission of S VOLCANOES" ;

EMI_S_WIF:long_name = "Emission of S WILDFIRE" ;

EMI_DMS:long_name = "Emission of DMS" ;

EMI_SO4_ANT:long_name = "Emission of SO4 ant" ;

EMI_SO4_NAT:long_name = "Emission of SO4 VOLCANOES" ;

EMI_SO4_WIF:long_name = "Emission of SO4 Wildfires" ;

EMI_BC:long_name = "Emission of BC" ;

EMI_OC:long_name = "Emission of OC" ;

EMI_SS:long_name = "Emission of SS" ;

EMI_SS_AS:long_name = "Emission of SS - Accumulation Mode" ;

EMI_SS_CS:long_name = "Emission of SS - Coarse Mode" ;

EMI_DU:long_name = "Emission of Dust" ;

EMI_DU_AI:long_name = "Emission of Dust - Accumulation Mode" ;

EMI_DU_CI:long_name = "Emission of Dust - Coarse Mode" ;

PROD_SO2_DMS_OH:long_name = "sulfur production gas phase via DMS+OH" ;

PROD_SO4_DMS_OH:long_name = "sulfate production gas phase via DMS+OH" ;

PROD_SO2_DMS_NO3:long_name = "sulfate production gas phase via DMS+NO3" ;

PROD_SO4_SO2_OH:long_name = "sulfate production gas phase via SO2+OH" ;

PROD_SO4_LIQ_ACC:long_name = "sulfate production liquid phase acc" ;

PROD_SO4_LIQ_COA:long_name = "sulfate production liquid phase coarse" ;

PROD_SO4_GAS:long_name = "sulfate production gas phase" ;

PROD_SO4_LIQ:long_name = "sulfate production liquid phase " ;

NUC_SO4:long_name = "nucleation of sulfate" ;

COND_SO4:long_name = "condensation of sulfate on aerosol" ;

SO4:long_name = "Mass mixing ratio SO4" ;

BC:long_name = "Mass mixing ratio BC" ;

OC:long_name = "Mass mixing ratio OC" ;

SS:long_name = "Mass mixing ratio SS" ;

DU:long_name = "Mass mixing ratio DU" ;

NUM_NS:long_name = "number mixing ratio - aerosol mode nucleation soluble" ;

NUM_KS:long_name = "number mixing ratio - aerosol mode aitken soluble" ;

NUM_AS:long_name = "number mixing ratio - aerosol mode accumulation soluble" ;

NUM_CS:long_name = "number mixing ratio - aerosol mode coarse soluble" ;

NUM_KI:long_name = "number mixing ratio - aerosol mode aitken insoluble" ;

NUM_AI:long_name = "number mixing ratio - aerosol mode accumulation insoluble" ;

NUM_CI:long_name = "number mixing ratio -aerosol mode coarse insoluble" ;

RWET_NS:long_name = "wet number median radius - NS" ;

RWET_KS:long_name = "wet number median radius - KS" ;

RWET_AS:long_name = "wet number median radius - AS" ;

RWET_CS:long_name = "wet number median radius - CS" ;

RWET_KI:long_name = "wet number median radius - KI" ;

RWET_AI:long_name = "wet number median radius - AI" ;

RWET_CI:long_name = "wet number median radius - CI" ;

TAU_SO4:long_name = "Optical thickness SO4 (550 nm)" ;

TAU_BC:long_name = "Optical thickness BC (550 nm)" ;

TAU_OC:long_name = "Optical thickness OC (550 nm)" ;

TAU_SS:long_name = "Optical thickness SS (550 nm)" ;

TAU_DU:long_name = "Optical thickness DU (550 nm)" ;

TAU_WAT:long_name = "Optical thickness WAT (550 nm)" ;

TAU_2D:long_name = "Optical thickness - total (550 nm)" ;

ABS_SO4:long_name = "Absorption optical thickness SO4 (550 nm)" ;

ABS_BC:long_name = "Absorption optical thickness BC (550 nm)" ;

ABS_OC:long_name = "Absorption optical thickness OC (550 nm)" ;

ABS_SS:long_name = "Absorption optical thickness SS (550 nm)" ;

ABS_DU:long_name = "Absorption optical thickness DU (550 nm)" ;

ABS_WAT:long_name = "Absorption optical thickness WAT (550 nm)" ;

ABS_2D:long_name = "Absorption optical thickness - total (0.55 um)" ;

ANG:long_name = "Angstroem parameter between 550 and 825 nm" ;

TAU_MODE_KS_3D:long_name = "Optical thickness (550 nm)" ;

TAU_MODE_AS_3D:long_name = "Optical thickness (550 nm)" ;

TAU_MODE_CS_3D:long_name = "Optical thickness (550 nm)" ;

TAU_MODE_KI_3D:long_name = "Optical thickness (550 nm)" ;

TAU_MODE_AI_3D:long_name = "Optical thickness (550 nm)" ;

TAU_MODE_CI_3D:long_name = "Optical thickness (550 nm)" ;

TAU_3D:long_name = "3D optical thickness at 550nm" ;

ABS_3D:long_name = "3D absorption optical thickness at 550nm" ;

TAU_MODE_KS:long_name = "Optical thickness (550 nm)" ;

ABS_MODE_KS:long_name = "Absorption optical thickness (550 nm)" ;

TAU_MODE_AS:long_name = "Optical thickness (550 nm)" ;

ABS_MODE_AS:long_name = "Absorption optical thickness (550 nm)" ;

TAU_MODE_CS:long_name = "Optical thickness (550 nm)" ;

ABS_MODE_CS:long_name = "Absorption optical thickness (550 nm)" ;

TAU_MODE_KI:long_name = "Optical thickness (550 nm)" ;

ABS_MODE_KI:long_name = "Absorption optical thickness (550 nm)" ;

TAU_MODE_AI:long_name = "Optical thickness (550 nm)" ;

ABS_MODE_AI:long_name = "Absorption optical thickness (550 nm)" ;

TAU_MODE_CI:long_name = "Optical thickness (550 nm)" ;

ABS_MODE_CI:long_name = "Absorption optical thickness (550 nm)" ;

srads:long_name = "net surface solar radiation" ;

srad0:long_name = "net top solar radiation" ;

srafs:long_name = "net surf. solar radiation   (clear sky)" ;

sraf0:long_name = "net top solar radiation   (clear sky)" ;

PRECIP:long_name = "Precipitation rate" ;